

RESEARCH

Open Access



Cell transplantation-mediated dystrophin supplementation efficacy in Duchenne muscular dystrophy mouse motor function improvement demonstrated by enhanced skeletal muscle fatigue tolerance

Clémence Kiho Bourgeois Yoshioka^{1,2}, Nana Takenaka-Ninagawa^{1,3*}, Megumi Goto¹, Mayuho Miki^{1,2}, Daiki Watanabe^{4,5}, Masamichi Yamamoto⁵, Tomoki Aoyama² and Hidetoshi Sakurai^{1*}

Abstract

Background Duchenne muscular dystrophy (DMD) is an incurable neuromuscular disease leading to progressive skeletal muscle weakness and fatigue. Cell transplantation in murine models has shown promise in supplementing the lack of the dystrophin protein in DMD muscles. However, the establishment of novel, long-term, relevant methods is needed to assess its efficiency on the DMD motor function. By applying newly developed methods, this study aimed to evaluate the functional and molecular effects of cell therapy-mediated dystrophin supplementation on DMD muscles.

Methods Dystrophin was supplemented in the gastrocnemius of a 5-week-old immunodeficient DMD mouse model (*Dmd*-null/NSG) by intramuscular xenotransplantation of healthy human immortalized myoblasts (Hu5/KD3). A long-term time-course comparative study was conducted between wild-type, untreated DMD, and dystrophin supplemented-DMD mouse muscle functions and histology. A novel GO-A⁺Team2 transgenic DMD mouse model was also generated to assess *in vivo* real-time ATP levels in gastrocnemius muscles during repeated contractions.

Results We found that 10.6% dystrophin supplementation in DMD muscles was sufficient to prevent low values of gastrocnemius maximal isometric contraction torque (MCT) at rest, while muscle fatigue tolerance, assessed by MCT decline after treadmill running, was fully ameliorated in 21-week-old transplanted mice. None of the dystrophin-supplemented fibers were positive for muscle damage markers after treadmill running, with 85.4% demonstrating the utilization of oxidative metabolism. Furthermore, ATP levels in response to repeated muscle contractions tended to improve, and mitochondrial activity was significantly enhanced in dystrophin supplemented-fibers.

Conclusions Cell therapy-mediated dystrophin supplementation efficiently improved DMD muscle functions, as evaluated using newly developed evaluation methods. The enhanced muscle fatigue tolerance in 21-week-old mice was associated with the preferential regeneration of damage-resistant and oxidative fibers, highlighting

*Correspondence:

Nana Takenaka-Ninagawa
nana.takenaka@cira.kyoto-u.ac.jp
Hidetoshi Sakurai
hsakurai@cira.kyoto-u.ac.jp

Full list of author information is available at the end of the article



© The Author(s) 2024. **Open Access** This article is licensed under a Creative Commons Attribution-NonCommercial-NoDerivatives 4.0 International License, which permits any non-commercial use, sharing, distribution and reproduction in any medium or format, as long as you give appropriate credit to the original author(s) and the source, provide a link to the Creative Commons licence, and indicate if you modified the licensed material. You do not have permission under this licence to share adapted material derived from this article or parts of it. The images or other third party material in this article are included in the article's Creative Commons licence, unless indicated otherwise in a credit line to the material. If material is not included in the article's Creative Commons licence and your intended use is not permitted by statutory regulation or exceeds the permitted use, you will need to obtain permission directly from the copyright holder. To view a copy of this licence, visit <http://creativecommons.org/licenses/by-nc-nd/4.0/>.

increased mitochondrial activity, after cell transplantation. These findings significantly contribute to a more in-depth understanding of DMD pathogenesis.

Keywords Duchenne muscular dystrophy mouse model, Cell transplantation, Dystrophin supplementation, Motor function evaluation, Muscle fatigue tolerance, Oxidative slow fibers, GO-ATeam2 transgenic mouse model, In vivo ATP imaging, Mitochondrial activity

Background

First described in the mid-1800s [1], Duchenne muscular dystrophy (DMD) is a rare, lethal inherited neuromuscular disease that affects 19.8/100,000 live male births [2]. Curative therapeutic development to treat DMD still intensively occupies scientific research [3]. Pathological manifestations such as muscular weakness and muscle fatigue develop progressively, and affected young children suffer from severe cardiac and motor function disorders that deteriorate cardiorespiratory and ambulatory functions [4]. Thousands of recessive genetic mutations have been identified in the X-linked *DMD* gene [5], which encodes the dystrophin protein [6], a component of the transmembrane dystrophin-associated protein complex (DAPC) in all (cardiac, skeletal, and smooth) muscle cells [7–9]. The chronic degeneration–regeneration cycles accompanied by accumulating damage and fibrosis described in the skeletal muscles of patients with DMD reportedly lead to global muscle atrophy [10, 11]. However, a precise understanding of the physiopathological mechanisms underlying DMD genesis is still unclear, and the adverse effects of dystrophin deficiency in the skeletal muscle sarcolemma on patients' functional deficits warrant further clarification.

Although steroid-based drug treatments associated with physical therapy are the gold standard for patients with DMD [12, 13], their use merely delays disease progression and causes inconvenient side effects [14, 15]. Among emerging therapeutic strategies [16], the safety of gene therapy is yet to be proven [17]. Although antisense-mediated exon-skipping restores dystrophin endogenous synthesis [18–21], it remains a personalized treatment due to *DMD* mutation variability [22]. Those two treatments are not completely curative as they are based on the production of a functional but shortened dystrophin protein [13]. In addition, regenerative medicine, which aims to overcome these issues, has shown promising results in the past decades; cell transplantation studies using muscle progenitor cells with normal dystrophin expression, which are derived from human or mouse models, are notably on the rise [23, 24]. They reported successful supplementation of full-length dystrophin protein in DMD mouse model muscles, as well as some improvements in muscle phenotype at the histological and/or functional levels [25–29]. Nevertheless, only a few

studies have reported the beneficial effects of transplantation therapies on muscle functional properties [30]. Therefore, this animal study aims to reliably demonstrate cell therapy-mediated dystrophin supplementation efficacy in DMD motor function.

The primary issue in previous studies lies in the methods used for muscle function assessment, which are diverse, such as *ex vivo* [25, 26, 28, 31] or *in situ* [32, 33] measurement of muscle tension, *in vivo* measurement of muscle contraction torque provoked by electrical stimulation [29], or more functional strength or exhaustion tests [28, 34]. Indeed, the major assessment scale used in ambulatory patients with DMD in clinical practice, the NorthStar Ambulatory Assessment (NSAA), not only considers muscular strength but also the functional aspects of patients' motor abilities, that is, outcomes that reflect DMD patients' functional abilities during their activities of daily living (ADL) [35]. Thus, to assess the effects of cell therapy on DMD motor function, the evaluation method should be specific to the analyzed muscle, repeatable in the same individual for time-course and disease progression assessment, reflect DMD muscle functional needs in ADL, and be suitable for clinical application. However, none of the above-mentioned methods, which have been reported thus far, could satisfy the required conditions simultaneously. Second, muscular strength and endurance tolerance functions work under distinct molecular mechanisms and endow each skeletal muscle with its role in the musculoskeletal system (for instance, most enduring muscles participate in posture or the respiratory system, while the strongest muscles participate in locomotion or prehension). However, the reported methods generally focus on muscle function without drawing a sufficient distinction between muscular strength, muscle fatigue tolerance, or the reasons for each assessment effect. Finally, although this is a well-known necessity for clinical applications, we underscored the absence of standardized, long-term functional evaluation protocols. Thus, considering the need for a novel, validated protocol to assess motor function abilities in a DMD mouse model before studying cell transplantation effects, we first conducted long-term experiments that combined the advantages of each existing method to establish an accurate and clinically relevant evaluation method for mouse muscle functions. To

this end, we also developed an effective transplantation method that supplements dystrophin protein in DMD mouse muscles. More precisely, we performed multiple intramuscular transplantations of human immortalized myoblasts (Hu5/KD3) [36] into the gastrocnemius muscles of a young immunodeficient NOD.Cg-Prkdc^{scid} Il2rg^{tm1Wjl}/SzJ (NSG) mouse model of DMD (*Dmd*-null/NSG) [29, 37].

Thereafter, we applied our newly established method to evaluate cell therapy-mediated dystrophin supplementation efficiency in DMD motor functions (maximal muscular strength and muscle fatigue tolerance). Although no significant improvement in maximal muscular strength was detected in this study, we found the minimal threshold required for the dystrophin supplementation rate to achieve a therapeutic effect. Furthermore, functional evaluations demonstrated a significant and long-term amelioration of muscle fatigue tolerance in dystrophin supplemented-DMD muscles. This functional enhancement was associated with the preferential regeneration of damage-resistant and oxidative myofibers with increased mitochondrial activity after cell therapy. These findings not only validate the treatment efficacy but further clarify the biomolecular pathogenic mechanisms that lead to DMD skeletal muscle functional phenotype.

Methods

Animal models

To prevent the immunological rejection of the human cell transplant, severely immunodeficient NOD.Cg-Prkdc^{scid} Il2rg^{tm1Wjl}/SzJ (NSG) mice were used. Immunodeficient wild type (WT)/NSG mice were purchased from Charles River Laboratories. The mice were mated with *Dmd*-null mice [37] to generate immunodeficient *Dmd*-null/NSG mice, as previously described by Zhao et al.

[29]. These mice were used as the DMD disease mouse model in this study. All WT and DMD mice were housed and bred under the same environmental conditions.

For the adenosine triphosphate (ATP) dynamics study, we used GO-ATeam2 transgenic C57BL/6 J male mice (paper under preparation), which enable ATP-level monitoring in living animals [38]. GO-ATeam2 is a fluorescent ATP probe developed by Nakano et al. [39], which uses green and orange fluorescent proteins as Förster resonance energy transfer (FRET) pairs. GO-ATeam2 heterozygous male mice were mated with immunodeficient NSG homozygous *Dmd*-null heterozygous female mice to create *Dmd*-null heterozygous females and WT male mice (both heterozygous for GO-ATeam2 and NSG), which were subsequently mated to create the GO-ATeam2 homozygous NSG homozygous *Dmd*-null (ATPtg *Dmd*-null/NSG) and WT (ATPtg WT/NSG) male mice used in further experiments. For genotyping, genomic DNA was extracted from mouse tails, and genomic PCR was performed using the Fw-Rv primer pairs listed in Table 1. We analyzed ATP levels in GO-ATeam2 transgenic mice after mouse generation and cell transplantation.

All animal experiments were reported in line with the ARRIVE (Animal Research: Reporting of In Vivo Experiments) guidelines 2.0.

Immortalized human myoblasts culture

Immortalized human Hu5/KD3 myoblasts [36] were provided by Dr. Naohiro Hashimoto (National Center for Geriatrics and Gerontology, Japan). They were cultured under 37 °C and 10% CO₂ conditions on 100 mm collagen type I-coated culture dishes (4020-010, Iwaki). The culture medium was Dulbecco's Modified Eagle Medium (DMEM; 08488-55, Nacalai Tesque) supplemented with

Table 1 List of primers used for genotyping

Target		Primer pairs	Predicted product size (base pairs)	
<i>Dmd</i>	Wild type	Fw	TGGGCAAGAGTGAATTTTCC	437
		Rv	ACCACCCACTTCAGGTTGAG	
	Knock-out	Fw	GAATTCAGCGAGAGCCTGAC	453
		Rv	GATGTTGGCGACCTCGTATT	
NSG	Wild type	Fw	GTGGGTAGCCAGCTCTTCAG	269
		Rv	CCTGGAGCTGGACAACAAT	
	Knock-out	Rv	GCCAGAGGCCACTTGTGTAG	349
GO-ATeam2	Wild type	Fw	ATTCTGCTTACATAGTCTAACTCGC	330
		Rv	TGGCAGGCTTAAAGGCTAA	
	Transgenic	Fw	AGAGCCTCTGCTAACCATGTTTCATGCCTTC	342
		Rv	GTGACACTAAGTCAAACGCGAAA	

0.5% penicillin–streptomycin mixed solution (09367-34, Nacalai Tesque), 1% L-glutamine (16948-04, Nacalai Tesque), 20% fetal bovine serum (554-02155 then 556-33865, Biosera), and 2% Ultrosor G (15950-017, Sartorius). Cells were passaged when they reached full confluence according to the following protocol: Cells were rinsed with Dulbecco's phosphate-buffered saline (D-PBS; 14249-24, Nacalai Tesque), detached, and dissociated into single cells by adding 2 mL of 2.5 g/L-trypsin/1 mmol/L-EDTA solution (35554-64, Nacalai Tesque) per dish, then centrifugated (190×g, 5 min, 4 °C), resuspended, counted, and seeded at density of $3\text{--}5 \times 10^5$ cells per dish. Frozen stocks were created in a Bamberker serum-free cryopreservation medium for long-term cell storage (CS-02-001, Nippon Genetics) to ensure experimental reproducibility.

Cell transplantation in DMD mouse model

After cell passages, cell suspensions containing $8\text{--}10 \times 10^6$ Hu5/KD3 cells (average) were centrifuged (200×g, 5 min, 4 °C), resuspended into 80–100 µL of fresh DMEM, and transferred in 1 mL 27Gx½ syringes (Myjector SS-10M2713, Terumo). Five-week-old *Dmd*-null/NSG mice were anesthetized by inhalation of 5% isoflurane (1119701G1084, AbbVie, M090AEC, MSD Animal Health K.K.). Their calves were shaved and cleaned with 70% ethanol. The transplantation protocol consisted of two longitudinal intramuscular injections of the Hu5/KD3 cell suspension parallel to the mouse calcaneal tendon in the middle third of each head of the right and left gastrocnemius muscles. Cell transplantation procedures were repeated twice weekly for 3 weeks, with a total of either five or six transplantation sessions, such that the average number of transplanted cells per muscle was adjusted to 50×10^6 cells. To prepare DMD mouse muscles in a regeneration-favorable environment and to maximize cell engraftment potential (paper under preparation), a muscle pre-conditioning exercise was conducted the day before one in two transplantation experiments. The protocol is described in detail in the following section.

Transcutaneous electrical stimulations on mouse skeletal muscles

Under 5% isoflurane (1119701G1084, AbbVie, M090AEC, MSD Animal Health K.K.) inhalation, calf-shaved mice were placed in the lateral decubitus position. The entire lower limb was blocked (knee joint at 60° and ankle joint at 90°), and the foot was fixed on a foot pressure sensor. One electrode (EK-1510SUS, Bio Research Center and PHT2R, Physio-Tech) was placed at the proximal extremity of the calcaneal tendon, and the other was placed 4.5 mm above, on the fleshy part of the gastrocnemius

muscle. Electrodes were connected to a biphasic electronic stimulator and an isolator (SEN-3401 and SS-203J, Nihon Kohden) according to the system designed by Itoh et al. [40], such that electrical stimulation resulted in tetanic isometric contraction of the triceps surae muscle. The ankle plantar flexion torque was transmitted from the sensor to a data logger (Midi Logger GL240, Graphtec Corporation) and analyzed using the associated software. 5 V stimuli were used for maximal contractions, and parameters were chosen following the results of Itoh et al. (100 Hz frequency, 1.0 ms duration, 650 ms train duration, and 5.0 mA current). The muscle pre-conditioning exercise before transplantation consisted of one set of 50 repeated isometric contractions (one contraction per second) at 40% of the maximal contraction torque, which was conducted by adjusting the stimulus current value. The parameters were set as follows: 40 Hz frequency, 2.0 ms duration, and 250 ms train duration.

Exercises to generate skeletal muscle fatigue in DMD mice

Two methods were used to induce muscle fatigue in the mouse triceps surae muscles. The first was chosen to be functional, using a 6-lane rodent treadmill (47300-001, Ugo Basile srl), and consisted of a 15 min horizontal constraint treadmill running at 9 m/min speed. The second was an electrical stimulation method used for the ATP imaging study. One set of 50 repeated isometric contractions (one contraction per second) at 10% of the maximal contraction torque to accustom the muscle to repeated contractions, followed by one set of 50 repeated isometric contractions (one contraction per second) at 40% of the maximal contraction torque to generate muscle fatigue, was performed on the gastrocnemius muscles of mice under anesthesia.

In vivo skeletal muscle function assessment outcomes

Muscle maximal-strength function was evaluated using electrically stimulated ankle plantar flexion maximal isometric contraction torque (MCT) assessment at rest. The average of two or three MCT values was used for a more accurate analysis.

Muscle fatigue function was evaluated by generating muscle fatigue according to the previous paragraph and by calculating the muscle fatigue ratio as follows: $\frac{MCT \text{ after muscle fatigue}}{MCT \text{ at rest}}$. As it required anesthesia, MCT at rest was assessed 1–2 days before the treadmill running session or the electrically stimulated repeated isometric contraction session, whereas “MCT after muscle fatigue” outcome was assessed right after the muscle-fatigue session. Mice that stopped running before 15 min because of dyspnea were excluded from the analysis.

Muscle harvest and muscle tissue sample preparation

Mice were euthanized by carbon dioxide gas inhalation right after the last functional evaluation.

For histological analysis, triceps surae muscles were harvested and fixed on cork stands using tragacanth gum (206-02242, Fujifilm Wako). They underwent quick deep freeze in 2-methylbutane (isopentane; 166-00615, Fujifilm Wako) cooled by liquid nitrogen for 1 min and were stored at -80°C for long-term preservation. Muscle samples were sectioned from proximal to distal in a cryostat (Leica CM 1850 and Leica CM 1950, Leica) to obtain 10–14- μm -thick slices on adhesive glass slides (APS-02, APS-03, APS-04, and APS-05, Matsunami). The central part of the muscle, characterized by the largest diameter, was visually identified; a 1.0–1.8 mm muscle portion was sectioned proximally, and a 300–400 μm was sectioned distally. Sample slides were stored at -80°C .

In view of electron microscopy analysis, mice triceps surae muscles were roughly sectioned with a blade and incubated at 4°C in the fixation liquid provided by Tokai Electron Microscopy Inc., which contained 2% paraformaldehyde, 2% glutaraldehyde in 0.1 M phosphate buffer (PB; pH 7.4). After overnight incubation at 4°C , samples were sent to Tokai Electron Microscopy Inc., which conducted further sample preparation steps, observation, imaging, and analysis. According to their protocol description, samples were rinsed, then secondary fixed with 2% osmium tetroxide in 0.1 M phosphate buffer for 2 h at 4°C . After dehydration in graded ethanol from 50 to 100%, the samples were placed twice in propylene oxide (PO) for 30 min at room temperature and then in a 7:3 mixture of PO and resin (Quetol-812, Nissin EM Co) for 1 h at room temperature. The day after, samples were embedded in fresh resin and heated for 48 h at 60°C . Ultrathin 70 nm sections were prepared by ultramicrotomy (Ultracut UCT, Leica) with diamond knives and copper grids.

To proceed to western blot analysis, mice triceps surae muscles were lysed in radioimmunoprecipitation assay (RIPA) buffer (08714-04, Nacalai Tesque) with protease inhibitor cocktail (25955-11, Nacalai Tesque) diluted in Milli-Q[®] ultrapure water (IQ 7005, Merck KGaA). First, muscle samples were quickly and carefully homogenized with Bio-Gen PRO2000 (PRO Scientific), then SDS solution (from the RIPA buffer set) was added, and sonication was applied during 4 min 30 s (15 s intervals) at 4°C (Bioruptor, Cosmo Bio Co). Muscle lysates were collected from supernatants after 15 min centrifugation (20,400 $\times g$) at 4°C and protein quantification was assessed using Pierce BCA assay kit (23227, Thermo Fisher Scientific) using an EnVision multilabel plate reader (2104, Perkin Elmer).

Fluorescent immunohistochemistry analysis

After muscle tissue sample preparation, the cryosections were stained according to the following protocol. After air-drying, they were fixed with acetone (00310-95, Nacalai Tesque) for 7 min at -30°C , washed twice with D-PBS (11482-15, Nacalai Tesque) for 5 min each, blocked with Blocking One solution (03953-95, Nacalai Tesque) for 1 h at room temperature, and incubated with the appropriate primary antibodies diluted in Can Get Signal immunostain Solution B (NKB-601, Toyobo) as referenced in Table 2. Primary antibodies were washed with D-PBS supplemented by 0.2% Triton X-100 (PBS-T; 35501-15, Nacalai Tesque) for 10 min for 3 times, then muscle tissue samples were incubated with the appropriate secondary antibodies and with DAPI (4',6-Diamidino-2-Phenylindole, Dihydrochloride) diluted in Can Get Signal immunostain Solution B (NKB-601, Toyobo) as referenced in Table 2. Secondary antibodies were washed once with PBS-T for 5 min and then twice with D-PBS for 5 min. Finally, muscle tissue samples were mounted with Vectashield antifade mounting medium with DAPI (H-1200, Vector Laboratories) under a protective microcover glass (No.1, Matsunami) and temporarily stored at 4°C under a light shield until analysis.

Myosin heavy chain type IIB was stained combining conventional immunohistochemistry with alkaline phosphatase (AP) enzyme-based coloration systems, according to the following steps: fixed muscle tissue samples underwent 15 min blocking with 10% normal goat serum (NGS) in PBS-T, overnight incubation with primary antibody diluted in 15% NGS in PBS-T (Table 2), washing, 45 min incubation with biotinylated secondary antibody, washing, 30 min incubation with Vectastain ABC-AP reagent (AK-50000, Vector Laboratories), washing, and a final 7-min incubation with ImmPact Vector Red AP substrate working solution (SK-5105, Vector Laboratories). For the last step, the red coloring reaction was monitored under a microscope and stopped by plunging the sample slides into Milli-Q[®] ultrapure water (IQ 7005, Merck KGaA). The previously described fluorescent immunostaining protocol was used to detect and analyze other proteins in the same samples.

Other histochemistry analysis

To study skeletal muscle damage, Evans blue dye (EBD; E2129-10G, Sigma-Aldrich) was dissolved in D-PBS (11482-15, Nacalai Tesque) to prepare a 10 mg EBD/mL D-PBS solution. Under 5% isoflurane (1119701G1084, AbbVie, M090AEC, MSD Animal Health K.K.) inhalation, 100 μL of EBD solution were intravenously injected in the mouse penile vein using 1 mL 27G $\times\frac{1}{2}$ syringe (Myjector SS-10M2713, Terumo), one day before the last functional evaluation and muscle harvest. EBD

Table 2 List of antibodies and dyes used for immunohistochemistry (IHC) and western blot (WB)

	Target molecule	Host species and isotype (clonality)	Dilution ratio	Incubation conditions	Reference
Primary antibodies	Human and mouse dystrophin	Rabbit IgG (polyclonal)	1: 200 (IHC) or 1: 500 (WB)	4 °C, 1 (IHC, WB) or 2 overnight (IHC)	ab15277, abcam
	Human and mouse Laminin-2 (α-2-chain)	Rat IgG1 (monoclonal)	1: 50 (IHC)	4 °C, 1 or 2 overnight (IHC)	ALX-804-190, Alexis
	Human and mouse myosin heavy chain type I	Mouse IgG2b (monoclonal)	1: 200 (IHC)	4 °C, overnight (IHC)	BA-D5, Developmental Studies Hybridoma Bank
	Human and mouse myosin heavy chain type IIA	Mouse IgG1 (monoclonal)	1: 200 (IHC)	4 °C, overnight (IHC)	SC-71, Developmental Studies Hybridoma Bank
	Mouse myosin heavy chain type IIB	Mouse IgM (monoclonal)	1: 200 (IHC)	4 °C, overnight (IHC)	BF-F3, Developmental Studies Hybridoma Bank
	Human, mouse and rat mitochondrial OXPHOS complexes (① <i>anti-CI subunit NDUFB8</i> ; ② <i>anti-CII-30 kDa</i> ; ③ <i>anti-CIII-Core protein 2</i> ; ④ <i>anti-CIV subunit I</i> ; ⑤ <i>anti-CV alpha subunit</i>)	① Mouse IgG1 (monoclonal) ② Mouse IgG2a (monoclonal) ③ Mouse IgG1 (monoclonal) ④ Mouse IgG2a (monoclonal) ⑤ Mouse IgG2b (monoclonal)	1: 1000 (WB)	4 °C, overnight (WB)	ab110413, abcam ① ab110242 ② ab14714 ③ ab14745 ④ ab14705 ⑤ ab14748
	Human, mouse and rat glyceraldehyde 3-phosphate dehydrogenase (GAPDH)	Mouse IgG1 (monoclonal)	1: 5000 (WB)	4 °C, overnight (WB)	MAB374, Millipore
Secondary antibodies	Rabbit IgG (H + L), Alexa Fluor® 488 conjugated	Goat IgG (polyclonal)	1: 500 (IHC)	Room temperature, 1 h (IHC)	A11034, Thermo Fisher Scientific
	Rabbit IgG (H + L), Alexa Fluor® 568 conjugated	Goat IgG (polyclonal)	1: 500 (IHC)	Room temperature, 1 h (IHC)	A11036, Thermo Fisher Scientific
	Rabbit IgG (H + L), peroxidase conjugated	Goat IgG (polyclonal)	1: 20,000 (WB)	Room temperature, 1 h (WB)	PI-1000, Vector Laboratories
	Rabbit IgG, biotinylated	Goat IgG (polyclonal)	1: 500 (IHC)	Room temperature, 1 h (IHC)	BA-1000, Vector Laboratories
	Rat IgG (H + L), Alexa Fluor® 647 conjugated	Goat IgG (polyclonal)	1: 500 (IHC)	Room temperature, 1 h (IHC)	A21247, Thermo Fisher Scientific
	Rat IgG (H + L), Alexa Fluor® 568 conjugated	Goat IgG (polyclonal)	1: 500 (IHC)	Room temperature, 1 h (IHC)	A11077, Thermo Fisher Scientific
	Rat IgG (H + L), Alexa Fluor® 488 conjugated	Goat IgG (polyclonal)	1: 500 (IHC)	Room temperature, 1 h (IHC)	A-11006, Thermo Fisher Scientific
	Mouse IgG2b (γ2b), Alexa Fluor® 488 conjugated	Goat IgG (polyclonal)	1: 500 (IHC)	Room temperature, 1 h (IHC)	A21141, Thermo Fisher Scientific
	Mouse IgG1 (γ1), Alexa Fluor® 488 conjugated	Goat IgG (polyclonal)	1: 500 (IHC)	Room temperature, 1 h (IHC)	A21121, Thermo Fisher Scientific
	Mouse IgM (mu chain specific), biotinylated	Goat IgG (polyclonal)	1: 100 (IHC)	Room temperature, 45 min (IHC)	BA-2020, Vector Laboratories
Mouse IgG, peroxidase conjugated	Horse	1: 20,000 (WB)	Room temperature, 1 h (WB)	PI-2000, Vector Laboratories	
DAPI	Adenine–thymine-rich regions in DNA	–	1: 5000 (IHC)	Room temperature, 1 h (IHC)	D1306 Thermo Fisher Scientific

macroscopically stains the damaged myofibers in blue [41]. To localize EBD at the cellular level, cryosections were observed under a fluorescence microscope equipped with 568 nm activation filters, as EBD emits

reddish fluorescence when exposed to green light. Thus, because damaged myofibers can be detected microscopically using red fluorescence, they could be studied in combination with other immunohistochemical protocols.

Muscle tissue samples were stained with hematoxylin (purple nuclei) and eosin (pink cytoplasm) for histological analysis. The fixed sample slides were plunged into Mayer's hemalum solution (1.09249.0500, Sigma-Aldrich) for 3 min, rinsed under a continuous water stream for 20 min, immersed in a 0.5% aqueous eosin Y solution (1.09844.1000, Sigma-Aldrich) for 6 min, and finally rinsed under a continuous water stream for 3 min. After 15 min air-drying, samples were mounted on a clean bench with one drop of Mount Quick (Daigo Sangyo) and protected using a micro-cover glass (No.1, Matsunami).

Fibrosis was studied by collagen type I and II staining under the following protocol: after 30 min of air-drying, the fixed samples were mounted with Picosirius Red F3BA (Solution B; 24901B-250, Polysciences Inc.) for 90 min, followed by 0.1 N hydrochloride acid (Solution C; 24901C-250, Polysciences Inc.) twice for 1 min. Thereafter, the slides were plunged into Milli-Q[®] ultrapure water (IQ 7005, Merck KGaA) for 1 s and into 70% ethanol (14712-05, Nacalai Tesque) in Milli-Q[®] ultrapure water for 30 s. After an additional 20 min of air-drying, the samples were mounted on a clean bench using one drop of Mount Quick (Daigo Sangyo) and protected using a micro-cover glass (No. 1, Matsunami).

Muscle samples were sent to Tokai Electron Microscopy Inc. for mitochondria observation using transmission electron microscopy (TEM). According to the manufacturer's protocol, ultrathin muscle samples sectioned by ultramicrotomy were placed in 2% uranyl acetate for 15 min at room temperature and stained with a lead stain solution (Sigma-Aldrich) for 3 min at room temperature.

Mitochondrial activity was analyzed in muscle tissue samples using reduced nicotinamide adenine dinucleotide-tetrazolium reductase (NADH-TR) oxidative enzyme staining, complementary to dystrophin staining. After air-drying, muscle tissue samples were incubated for 30 min at 37 °C with β -nicotinamide adenine dinucleotide (N8129, Sigma-Aldrich) and nitro blue tetrazolium (D0844, Tokyo Chemical Industry) diluted in 0.05 M Tris-HCl buffer (35436-01, Nacalai Tesque). The reaction was stopped by successive quick immersion in 60%, 90%, 60%, and 0% acetone (00310-95, Nacalai Tesque) in Milli-Q[®] ultrapure water (IQ 7005, Merck KGaA). Dystrophin was then stained using the AP enzyme-based coloration method to detect red fluorescence, as described in the previous paragraph. Finally, after washing for 5 min and air-drying for 5 min, the samples were mounted with Aqua-Poly/Mount solution (18606-20, Polysciences Inc.) under a protective micro-cover glass (No. 1, Matsunami) and stored at room temperature until analysis.

Western blot analysis

For western blot analysis, proteins from muscle lysates (preparation described in previous paragraph; 100 μ g for dystrophin detection, 20 μ g for mitochondrial complexes) were mixed with 10% NuPAGE sample reducing agent (10 \times ; NP0004, Thermo Fisher Scientific), 25% NuPAGE LDS sample buffer (4 \times ; NP0007, Thermo Fisher Scientific), and Milli-Q[®] ultrapure water (IQ 7005, Merck KGaA). After protein denaturation (except for mitochondrial complexes), muscle lysates were loaded with Protein Ladder One Plus (19,593–25, Nacalai Tesque) in NuPAGE 3–8% Tris-Acetate gels (NW04122BOX, Thermo Fisher Scientific) for dystrophin detection or in Bolt 4–12% Bis-Tris Plus gels (EA0375BOX, Thermo Fisher Scientific) for mitochondrial complex detection. A mitochondrial extract from rat heart tissue lysate (ab110341, Abcam) was used as a positive control (1/50 was loaded compared to other samples lanes) and glyceraldehyde 3-phosphate dehydrogenase (GAPDH) was selected as a housekeeping protein for mitochondrial complex detection. Protein separation by electrophoresis was conducted in mini-gel tanks (A25977, Thermo Fisher Scientific) with the corresponding SDS running buffer (LA0041 or B0002, Thermo Fisher Scientific) under the following settings: 150 V, 300 mA, 60 min. Dry transfer was performed on PVDF membranes (IB401002, Thermo Fisher Scientific) using an iBlot gel transfer device (IB1001 or IB21001, Thermo Fisher Scientific). After rinsing with Tris-buffered saline (TBS; 12748-31, Nacalai Tesque) supplemented with 0.05% Triton X-100 (TBS-T; 35501-15, Nacalai Tesque), the membranes were blocked with Blocking One solution (03953-95, Nacalai Tesque) for 1 h at room temperature and incubated with the appropriate primary antibodies diluted in Can Get Signal immunoreaction enhancer solution 1 (NKB-101, Toyobo) as referenced in Table 2. Primary antibodies were washed with TBS-T for 10 min 3 times, then the membranes were incubated with the appropriate secondary antibodies diluted in Can Get Signal immunoreaction enhancer solution 2 (NKB-301, Toyobo), as shown in Table 2, and washed again with TBS-T for 10 min 3 times. Membranes were mounted with SuperSignal West Femto Maximum Sensitivity Substrate (34094 or 34095, Thermo Fisher Scientific), and proteins were detected using Amersham ImageQuant 800 (IG800, Cytiva) in chemiluminescence mode. After imaging, membranes were washed and stained with Coomassie brilliant blue staining (CBB; 11642-31, Nacalai Tesque) for 5 min, rewashed with Milli-Q[®] ultrapure water (IQ 7005, Merck KGaA), and dried. A second detection in colorimetric mode was performed to evaluate the total protein amount per lane. Quantitative analysis after western blot experiments was conducted using ImageJ

software, and the ratios of the proteins of interest were normalized to the ratios of the total detected proteins.

In vivo live imaging of ATP levels

ATP imaging experiments were performed in the Yamamoto Laboratory (National Cerebral and Cardiovascular Center, Osaka, Japan) equipped with a fluorescence macro-microscope for live imaging, as described by Choi et al. [42]. Under anesthesia, one leg of the mice was attached to a home-made foot holder connected to a force transducer. Thereafter, gastrocnemius muscle was exposed, placed under the objective lens, and electrically stimulated via skin electrodes attached parallelly to the muscle long axis. Ten images per second of ATPtg *Dmd*-null/NSG (randomly transplanted into the right or left leg) and ATPtg WT/NSG mouse gastrocnemius muscles were captured while undergoing muscle fatigue created by electrically stimulated repeated isometric contractions. The detailed protocol for repeated contractions and electrical stimulation parameters has been described in the previous paragraphs.

Image analysis

Stained muscle tissue samples were examined under a confocal laser scanning microscope (LSM710, Zeiss) and then imaged with a 10× objective for quantitative analysis (HS All-in-one fluorescence microscope BZ-X700 or BZ-X710, Keyence) and a 20× objective to obtain higher quality images for qualitative analysis (LSM900, Zeiss and BZ-X800, Keyence). Quantitative analysis was performed using the BZ-X Analyzer software (Keyence). For dystrophin and EBD analyses, 2 slides were selected for each DMD muscle (1 for WT muscles) at less than 50 μm proximo-distal from the middle of the muscle. The number of dystrophin-supplemented myofibers and EBD-positive muscle cross-sectional area (CSA) were analyzed, and the maximal value was retained as measurement. Myosin heavy chain staining for myofiber-type analysis was performed on slides that were proximodistally close to the slide with the highest number of dystrophin-positive fibers out of the two previously counted. Laminin analysis was performed to study single myofiber CSA, minor axis, number, whole muscle tissue CSA, total muscle CSA, and ratio calculations. The staining intensity of NADH-TR was analyzed using BZ-X Analyzer software (Keyence). For electron microscopy analysis, lead-stained muscle tissue samples were imaged using a transmission electron microscope (100 kV of acceleration voltage; JEM-1400Plus, JEOL Ltd.) equipped with a CDD camera (EM-14830RUBY2, JEOL Ltd.) by Tokai Electron Microscopy, Inc. ATP imaging was performed using MetaMorph software (Molecular Devices, USA), as described by Choi et al. [38, 42]. The time-point for

ATP-level evaluation at rest was chosen just before the start of repeated muscle contractions, while the time-point for ATP-level evaluation after muscle fatigue was chosen after the stop of the contraction session, just before “MCT after muscle fatigue” was evaluated. The ATP level ratio was calculated as follows:

$$\frac{\text{ATP level after muscle fatigue}}{\text{ATP level at rest}}$$

Statistical analysis

Data are presented as the mean ± standard error of the mean (SEM). In the column graphs, the number indicated at the top and bottom of the columns represent the data value and sample size, respectively. Statistical comparison between three groups (mostly for WT, untreated DMD, and dystrophin supplemented-DMD mice) or more was performed by one-way analysis of variance (ANOVA) followed by a multiple comparisons test using post-hoc Tukey honestly significant difference test on Prism 9 or Prism 10 software (GraphPad). Statistical comparisons between the two groups were performed using the Student's t-test. Spearman's correlation test, Shapiro–Wilk normality test, and receiver operating characteristic (ROC) curve analysis were performed using modified R Commander software (EZR version from Jichi Medical University Saitama Medical Center, Japan) to clarify the link between the number of dystrophin-supplemented fibers and functional outcomes. A *p*-value of less than 5% was considered statistically significant for all statistical analyses. In the figures, “*” indicates $0.01 \leq p < 0.05$, “**” $0.001 \leq p < 0.01$, “***” $0.0001 \leq p < 0.001$, and “****” $p < 0.0001$; “N.S.” indicates that the difference was not statistically significant.

Results

Differences in the long-term functional effects of cell therapy-mediated dystrophin supplementation

To study the effects of dystrophin supplementation on DMD motor function in a murine model, an average of $4.10^7/6.10^7$ Hu5/KD3 cells with normal dystrophin expression were transplanted into the gastrocnemius muscles (half in each head) of 5–7-week-old (wo) *Dmd*-null/NSG mice (Fig. S1A). A long-term comparative study of two types of muscle functions was conducted with three mice groups: untreated DMD, dystrophin supplemented-DMD, and WT mice. The first type of evaluated function was muscular strength. Electrically stimulated plantar flexion MCT at rest was assessed in mice once every four weeks from 13 to 33 weeks of age. Statistically significant decline of MCT was accurately reflected in DMD mice from 13 to 33 weeks of

age ($6.19 \text{ mNm} \pm 0.15$ and $5.13 \text{ mNm} \pm 0.12$ respectively) compared to WT mice ($7.41 \text{ mNm} \pm 0.19$ and $7.42 \text{ mNm} \pm 0.19$ respectively). However, MCT at rest was comparable in untreated DMD and dystrophin supplemented-DMD mice groups from 13 to 33 weeks of age ($6.46 \text{ mNm} \pm 0.16$ and $5.20 \text{ mNm} \pm 0.29$, respectively; Fig. 1A). MCT normalized to mouse body weight (MCT/BW ratio) revealed comparable results (Fig. 1B). Since the data did not change with or without weight normalization, further results were described without normalization.

The second type of evaluated function was muscle fatigue, which is defined as a weakness that occurs upon repetitive muscle use. The treadmill running (TMR) method was chosen to induce muscle fatigue in the mouse legs, and MCT was measured again immediately after running. This muscle fatigue assessment was repeated once every four weeks from 13 to 21 weeks of age. Several running speeds and duration parameters were considered: 15 min horizontal TMR at 9 m/min (method A; Fig. 1C), 15 min horizontal TMR at 5 m/min (method B), and 8 min horizontal TMR at 9 m/min (method C). As method B did not accurately reflect DMD muscle fatigue phenotype compared to WT mice (Fig. S1B) and as method C did not detect any amelioration in dystrophin supplemented-DMD muscles compared to untreated DMD muscles (Fig. S1C), they were not adopted for further study. As for method A, MCT after TMR was significantly lower in untreated DMD mice from 13 to 21 weeks of age ($5.09 \text{ mNm} \pm 0.26$ and $4.86 \text{ mNm} \pm 0.18$ respectively) compared to WT mice ($6.12 \text{ mNm} \pm 0.26$ and $7.63 \text{ mNm} \pm 0.21$ respectively), and significantly higher in 17- and 21-week dystrophin supplemented-DMD mice ($5.81 \text{ mNm} \pm 0.30$ and $5.96 \text{ mNm} \pm 0.30$ respectively) compared to untreated DMD mice ($4.81 \text{ mNm} \pm 0.23$ and $4.86 \text{ mNm} \pm 0.18$ respectively; Fig. 1D). Likewise, the

ratio between MCT after TMR and MCT at rest (further named “muscle fatigue ratio”), which has the advantage of eliminating individual differences between mice, was significantly lower in 21-week untreated DMD mice (0.84 ± 0.03) compared to WT mice (1.07 ± 0.04), and significantly higher in 21-week dystrophin supplemented-DMD mice (1.11 ± 0.08) compared to untreated DMD mice (Fig. 1E). In addition, no statistical difference was observed between WT and dystrophin supplemented-DMD mice at 21 weeks of age (Fig. 1E). To validate these results in the even longer term, MCT after TMR and muscle fatigue ratio were measured in 33-week mice and were found significantly lower in untreated DMD mice compared to WT; a trend of amelioration was observed in dystrophin supplemented-DMD mice compared to untreated DMD mice (Fig. S1D, E). Furthermore, to verify that TMR evaluation itself had no influence on functional results, the previous functional outcomes were compared between mice that ran once every four weeks between 9 and 21 weeks of age and mice control, which were sedentary until evaluation at 21 weeks of age (Fig. 1F). In both the WT and DMD groups, no statistical difference was found between running and control mouse muscle functions, either for MCT after TMR (Fig. 1G) or muscle fatigue ratio (Fig. 1H). These results demonstrate that TMR evaluation itself did not affect muscle functional outcomes; therefore, the transplantation of dystrophin-expressing cells directly resulted in the amelioration of muscle fatigue tolerance in DMD mice.

Severe DMD muscle weakness phenotype prevented by cell therapy-mediated dystrophin supplementation

To confirm the successful supplementation of dystrophin protein in DMD skeletal muscles after cell transplantation and to proceed to quantitative analysis, mouse muscles were harvested after the last functional evaluation,

(See figure on next page.)

Fig. 1 Long-term effects of cell therapy-mediated dystrophin supplementation on DMD motor functions. **A** Plantar flexion maximal isometric contraction torque (MCT) of 13–33-week-old (wo) wild type (WT), untreated DMD (DMD) and dystrophin supplemented-DMD (DMD+Dys) mouse gastrocnemius assessed at rest. 13-wo: n = 72 (WT), n = 83 (DMD), n = 33 (DMD+Dys). 17-wo: n = 83 (WT), n = 83 (DMD), n = 39 (DMD+Dys). 21-wo: n = 100 (WT), n = 105 (DMD), n = 43 (DMD+Dys). 25-wo: n = 55 (WT), n = 55 (DMD), n = 25 (DMD+Dys). 29-wo: n = 44 (WT), n = 54 (DMD), n = 18 (DMD+Dys). 33-wo: n = 60 (WT), n = 64 (DMD), n = 20 (DMD+Dys). **B** MCT normalized to body weight (BW) of 13–33-week-old WT, DMD and DMD+Dys mouse gastrocnemius assessed at rest. Sample sizes: cf. **A** except for 33-wo, n = 62 (DMD). **C** Schematic representation of the time-course comparative study between 13 and 21-week WT, DMD and DMD+Dys mice. Lower panels represent functional and molecular analyses procedures. **D** MCT of 13–21-week WT, DMD and DMD+Dys mouse gastrocnemius assessed after treadmill running (TMR). 13-wo: n = 33 (WT), n = 37 (DMD), n = 12 (DMD+Dys). 17-wo: n = 29 (WT), n = 32 (DMD), n = 14 (DMD+Dys). 21-wo: n = 41 (WT), n = 47 (DMD), n = 17 (DMD+Dys). **E** Muscle fatigue ratio of 13–21-week WT, DMD and DMD+Dys mouse gastrocnemius assessed after TMR. Sample sizes: cf. **D**. **F** Schematic representation of the study of repeated functional assessments effects on DMD muscle functions. WT (WT+4TMR) and DMD (DMD+4TMR) mice that ran 4 times from 9 to 21-week were compared to WT (WT+1TMR) and DMD (DMD+1TMR) mice that underwent only one assessment at 21-week. **G** MCT of 21-week WT+1TMR, WT+4TMR, DMD+1TMR, DMD+4TMR mouse gastrocnemius assessed after TMR. n = 24 (WT+1TMR), n = 13 (WT+4TMR), n = 19 (DMD+1TMR), n = 14 (DMD+4TMR). **H** Muscle fatigue ratio of 21-week WT+1TMR, WT+4TMR, DMD+1TMR, DMD+4TMR mouse gastrocnemius assessed after TMR. Sample sizes: cf. **G**. Data are shown as mean \pm SEM. * $0.01 \leq p < 0.05$, ** $0.001 \leq p < 0.01$, *** $0.0001 \leq p < 0.001$, **** $p < 0.0001$, N.S. not significant

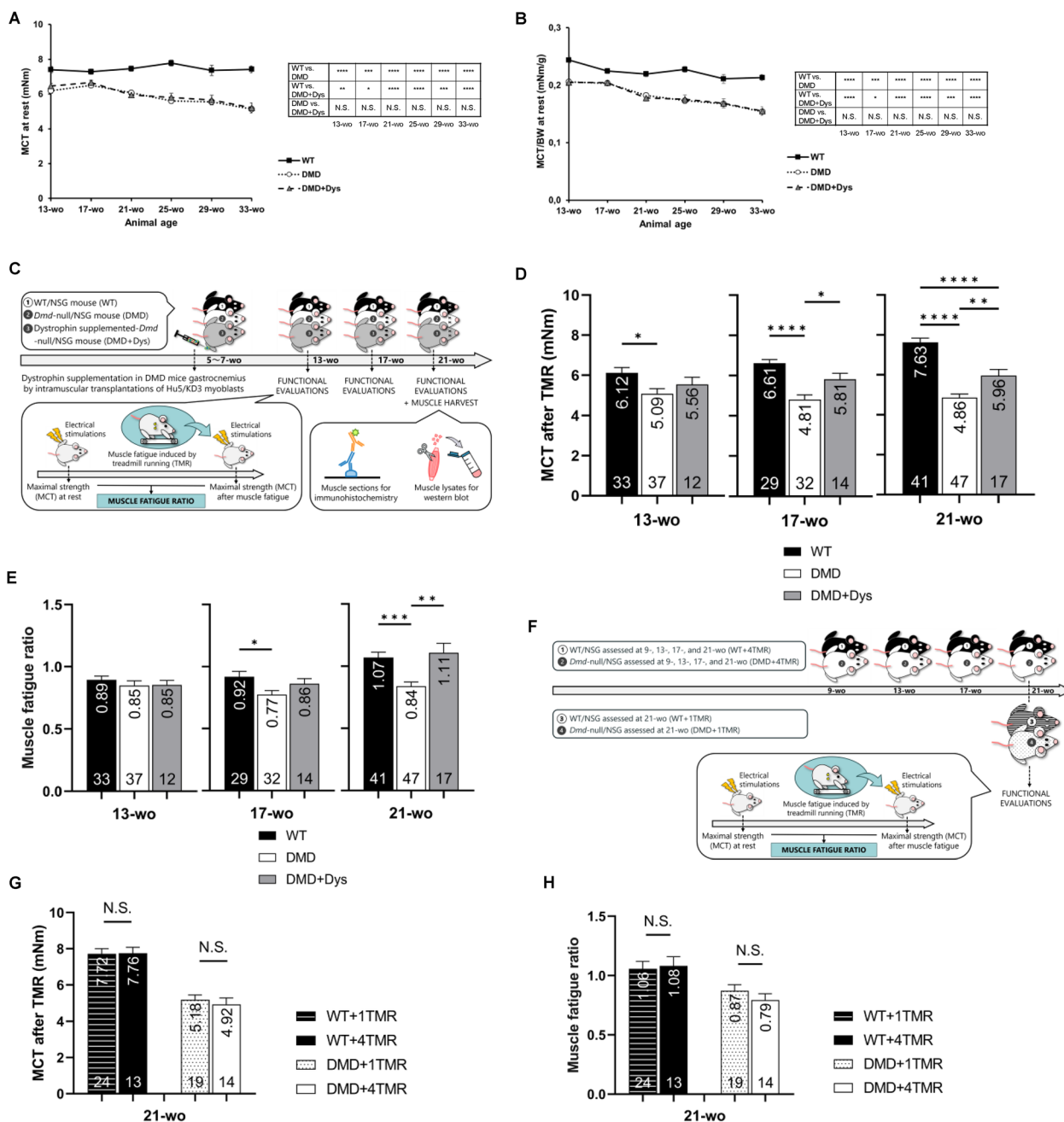


Fig. 1 (See legend on previous page.)

and cross-sectional muscle tissue samples were prepared for immunohistochemistry (Fig. 2A) or muscle lysates for protein detection by western blotting (Figs. 2B, S2A, B). The number of dystrophin-supplemented fibers in 21-wo mice muscle samples (1213 ± 234 average) and their percentage in the total number of myofibers ($10.6\% \pm 2.1$ average), here named “dystrophin supplementation rate” were calculated from stained sample images of whole gastrocnemius muscles (Fig. S2C). Statistical correlation

analyses were performed with data from over 21-wo mice in order to explain the differences previously discovered in the functional effects of dystrophin supplementation on DMD muscles (no impact on MCT but full recovery of muscle fatigue ratio). Spearman’s rank-order correlation coefficient showed a significant positive correlation ($r=0.54$) between the number of dystrophin-supplemented myofibers and mice MCT at rest (Fig. 2C). After confirming that MCT values were normally

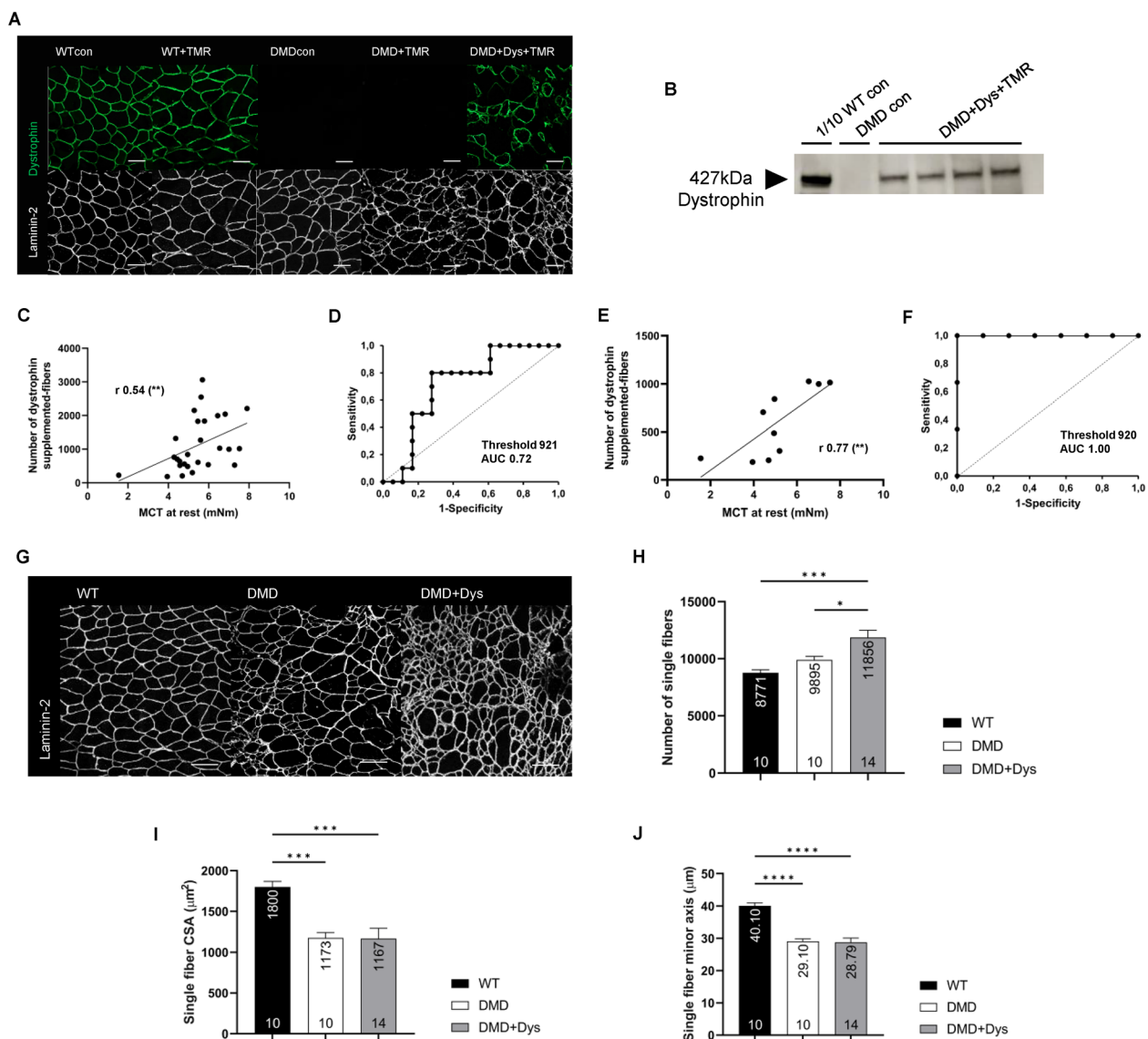


Fig. 2 Severe DMD muscle weakness phenotype prevented by cell therapy-mediated dystrophin supplementation. **A** Sectional immunostaining images of 21-week-old (wo) wild type (WT+TMR), untreated DMD (DMD+TMR) and dystrophin supplemented-DMD (DMD+Dys+TMR) mouse gastrocnemius collected after treadmill running (TMR) assessment. WT (WTcon) and DMD (DMDcon) control mice did not undergo functional assessment. Dystrophin (green) and laminin-2 (white) were stained to analyze dystrophin supplementation in DMD muscles after cell transplantation. Scale bars: 50 μm . **B** Cropped western blot of dystrophin in 21-wo DMD+Dys+TMR mouse gastrocnemius samples collected after TMR assessment. WTcon (positive control) and DMDcon (negative control) are samples from mice that did not undergo functional assessment. The full-length blot and Coomassie brilliant blue-stained blot used as control are presented in Supplementary Fig. 2. **C** Spearman's correlation between the number of dystrophin-supplemented fibers in DMD mouse gastrocnemius and plantar flexion maximal isometric contraction torque (MCT) assessed at rest. $r = 0.54$. $**p = 0.003$. $n = 28$. **D** Threshold of 921 dystrophin-supplemented DMD fibers revealed by the receiver operating characteristic (ROC) curve analysis. Area under the curve, AUC = 0.72. $n = 28$. **E** Spearman's correlation between the number of dystrophin-supplemented fibers in 33-wo DMD mouse gastrocnemius and MCT assessed at rest. $r = 0.77$. $**p = 0.009$. $n = 10$. **F** Threshold of 920 dystrophin-supplemented DMD fibers revealed by the ROC curve analysis in 33-wo mice samples. AUC = 1.00. $n = 10$. **G** Sectional immunostaining images of 21-wo wild type (WT), untreated DMD (DMD) and dystrophin supplemented-DMD (DMD+Dys) mouse gastrocnemius collected after TMR assessment. Laminin-2 (white) was stained to detect myofiber basal lamina. Scale bars: 100 μm . **H** Quantification of the number of single fibers from images in **G**. $n = 10$ (WT), $n = 10$ (DMD), $n = 14$ (DMD+Dys). **I** Quantification of single fiber cross-sectional area (CSA) from images in **G**. Sample sizes: cf. **H**. **J** Quantification of single fiber minor axis from images in **G**. Sample sizes: cf. **H**. Data are shown as mean \pm SEM. $*0.01 \leq p < 0.05$, $**0.001 \leq p < 0.01$, $***0.0001 \leq p < 0.001$, $****p < 0.0001$

distributed (p -value > 0.05) in the WT mouse population at each time-point by applying the Shapiro–Wilk normality test (Fig. S2D), 95% of WT mice MCT values were found > 4.47 mNm, > 3.50 mNm, and > 4.49 mNm at 21, 29, and 33 weeks of age, respectively. To establish the lower limit to consider a DMD mouse MCT value as normal, we set even higher thresholds: we calculated that 68% of WT mice MCT values were > 5.97 mNm at 21-wk, > 5.43 mNm at 29-wk and > 5.96 mNm at 33-wk. Using these thresholds for strength normality, further analysis of the ROC curve successfully indicated that 921 dystrophin-positive myofibers, corresponding to less than 10.6% supplementation, were sufficient for a DMD mouse to display a normal MCT value (area under the curve, AUC = 0.72; Fig. 2D).

The absence of functional improvement in the dystrophin supplemented-DMD mice group was first attributed to the lack of highly dystrophin-supplemented samples in this study. To confirm this hypothesis, analysis of maximal muscular strength at rest was performed again, with the exclusive inclusion of samples with more than 1000 (Fig. S2E), 1500 (Fig. S2F), or 2000 (Fig. S2G) dystrophin-supplemented myofibers after transplantation. Results tended to show a higher MCT at rest in dystrophin supplemented-DMD mice compared to untreated DMD mice, reaching WT mice levels; however, the p -value could not confirm statistically significant results due to the small number of samples (for instance, no sample with more than 1500 dystrophin-supplemented fibers remained at 33 weeks of age). Spearman's rank-order correlation analysis was then performed with the exclusive inclusion of 33-wk mice samples, revealing that the number of dystrophin-supplemented myofibers and mice MCT at rest were not only significantly but also more strongly correlated ($r = 0.77$; Fig. 2E). In addition, ROC curve analysis performed with MCT values of 33-wk mice indicated a higher AUC (Fig. 2F), supporting a stronger probability that comparable 920 dystrophin-supplemented fibers threshold was sufficient to prevent DMD low values of MCT and thus severe weakness phenotype.

In addition, as myofiber strength is related to myofiber diameter [43], immunofluorescent staining analysis of laminin protein subunit alpha 2 (laminin-2) was performed on cross-sectional muscle tissue samples from 21-wk mice (Fig. 2G). Results indicated that myofibers were more numerous in dystrophin supplemented-DMD muscles ($11,856 \pm 639$) than in both WT (8771 ± 260) and untreated DMD (9895 ± 316) muscles (Fig. 2H). However, the CSA of each single fiber was smaller in both untreated and supplemented DMD muscles ($1173 \mu\text{m}^2 \pm 66$ and $1167 \mu\text{m}^2 \pm 126$, respectively) compared to WT ($1800 \mu\text{m}^2 \pm 69$; Fig. 2I). The small size of myofibers in

both DMD groups muscles was confirmed by the analysis of their minor diameter, respectively $29.10 \mu\text{m} \pm 0.74$ and $28.79 \mu\text{m} \pm 1.33$ in untreated and transplanted DMD muscles (Fig. 2J). These results suggested that in addition to the number of dystrophin-supplemented DMD fibers, the small size of these regenerating fibers could also play a part in the absence of functional improvement of DMD muscular strength.

DMD muscle fatigue amelioration after dystrophin supplementation, favored by the protective role of dystrophin against muscle damage

The previous Spearman correlation test was performed again between the number of dystrophin-supplemented myofibers and muscle fatigue outcomes. Contrary to MCT at rest, the number of dystrophin-supplemented myofibers was not correlated with MCT after TMR or with muscle fatigue ratio (Fig. 3A, B). Therefore, muscle tissue structure was observed to investigate other biomolecular mechanisms that could account for the amelioration of DMD muscle-fatigue tolerance after cell transplantation-mediated dystrophin supplementation. Qualitative image analysis of hematoxylin and eosin-stained cross-sectional samples suggested that muscle degeneration was reduced in DMD muscles after dystrophin supplementation compared to that in untreated DMD muscles, as a decrease in necrotic fibers was observed (Fig. 3C). Moreover, the ratio of total myofibers CSA in total muscle CSA tended to be higher in dystrophin supplemented-DMD myofibers ($65.6\% \pm 1.4$) than in untreated DMD myofibers ($61.0\% \pm 2.6$; Fig. 3D). Along with these results, Picrosirius red staining brought similar results concerning muscle fibrosis that was significantly reduced in dystrophin supplemented-DMD muscles ($2,256,314 \mu\text{m}^2 \pm 391,633$) compared to untreated DMD muscles ($4,232,720 \mu\text{m}^2 \pm 434,569$; Fig. 3E).

These findings led to a more detailed study of the damage in DMD skeletal muscles that have undergone muscle fatigue by TMR. EBD was systemically injected into the mouse penile vein the day before the last TMR evaluation and muscle harvest to study degenerating myofibers (Fig. S3A). On the one hand, muscle tissue cross-sectional samples analysis revealed that EBD-positive CSA was significantly higher in DMD muscles after TMR ($1,325,645 \mu\text{m}^2 \pm 197,782$) than in DMD sedentary control muscles ($586,687 \mu\text{m}^2 \pm 99,780$; Fig. 3F). However, it was comparable in both running and sedentary control WT muscles ($10,192 \mu\text{m}^2 \pm 4681$ and $6419 \mu\text{m}^2 \pm 1762$, respectively), indicating that TMR caused myofiber damage only in DMD muscles. On the other hand, EBD-positive CSA after TMR was significantly reduced in dystrophin supplemented-DMD muscles ($625,619 \mu\text{m}^2 \pm 110,484$) compared to untreated

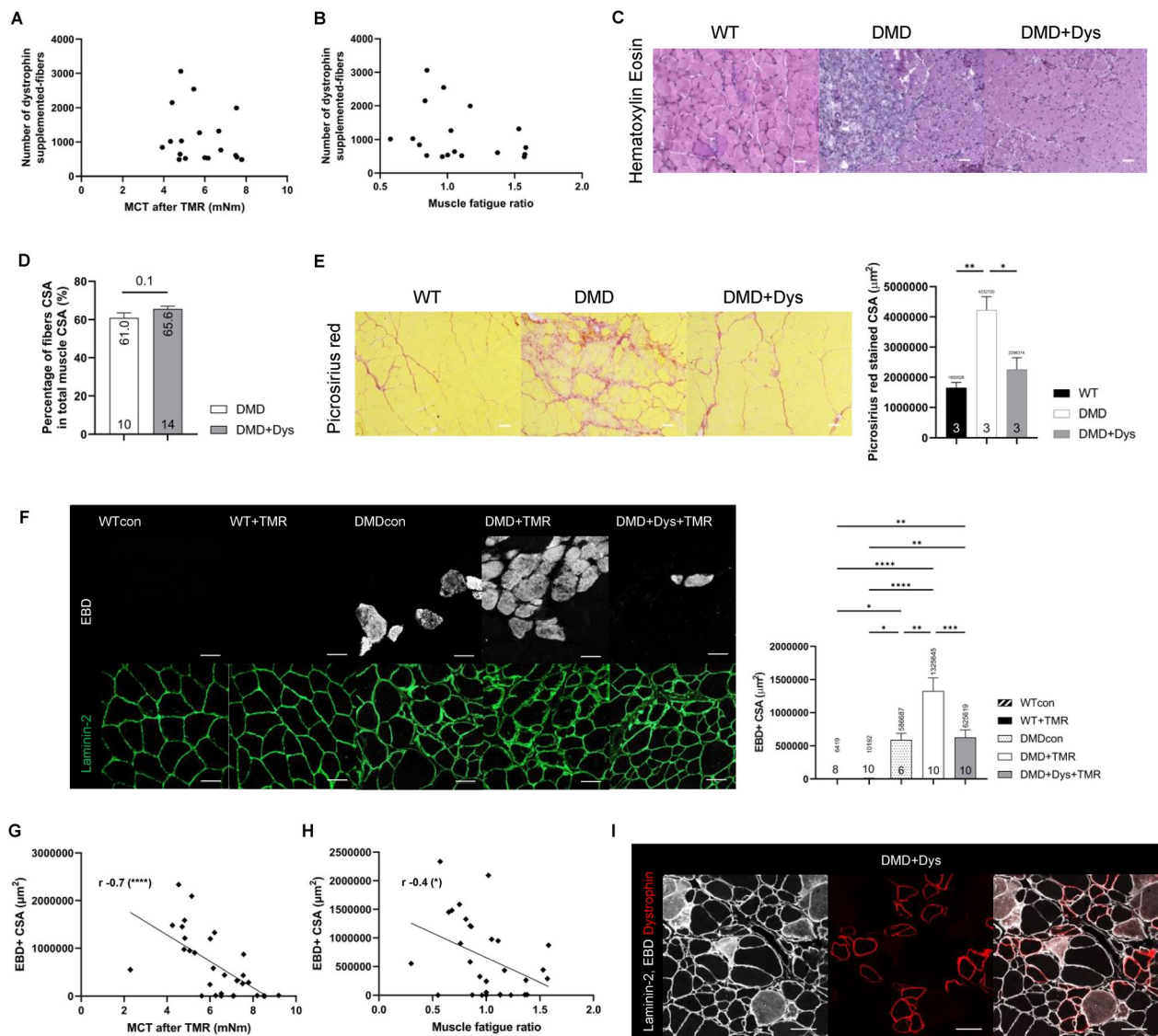


Fig. 3 Dystrophin protective role against muscle damage. **A** No correlation between the number of dystrophin-supplemented fibers in 21-week-old (wo) DMD mouse gastrocnemius and plantar flexion maximal isometric contraction torque (MCT) assessed after treadmill running (TMR). $r = -0.25$, $p = 0.31$, $n = 18$. **B** No correlation between the number of dystrophin-supplemented fibers in 21-wo DMD mouse gastrocnemius and muscle fatigue ratio assessed after TMR. $r = -0.28$, $p = 0.26$, $n = 18$. **C** Sectional images of gastrocnemius of 21-wo wild type (WT), untreated DMD (DMD) and dystrophin supplemented-DMD (DMD + Dys) mice collected after TMR assessment, stained with hematoxylin (purple nuclei) and eosin (pink cytoplasm). Scale bars: 50 μ m. **D** Total fiber per total muscle cross-sectional area (CSA) ratio, reflecting the proportion of the muscle tissue. $p = 0.1$, $n = 10$ (DMD), $n = 14$ (DMD + Dys). **E** Sectional images of gastrocnemius of 21-wo WT, DMD and DMD + Dys mice collected after TMR assessment, stained with Picrosirius red. Scale bars: 50 μ m. Quantitative graph shows fibrosis CSA. $n = 3$. **F** Sectional images of gastrocnemius of 21-wo wild type (WT + TMR), untreated DMD (DMD + TMR) and dystrophin supplemented-DMD (DMD + Dys + TMR) mice collected after TMR assessment. WT (WTcon) and DMD (DMDcon) control mice did not undergo functional assessment. Myofiber damage was stained by Evans blue dye (EBD; white) and laminin-2 (green) detected basal lamina. Scale bars: 50 μ m. Quantitative graph shows EBD-positive CSA (EBD + CSA). $n = 8$ (WTcon), $n = 10$ (WT + TMR), $n = 6$ (DMDcon), $n = 10$ (DMD + TMR), $n = 10$ (DMD + Dys + TMR). **G** Spearman's correlation between EBD + CSA and MCT of 21-wo mouse gastrocnemius assessed after TMR. $r = -0.7$, **** $p < 0.0001$, $n = 30$. **H** Spearman's correlation between EBD + CSA and muscle fatigue ratio of 21-wo mouse gastrocnemius assessed after TMR. $r = -0.4$, * $p = 0.03$, $n = 30$. **I** Sectional images of gastrocnemius of 21-wo DMD + Dys mice collected after TMR assessment. Fibers positive for both EBD (white CSA) and dystrophin (red membrane) were evaluated. Scale bars: 50 μ m. Data are shown as mean \pm SEM. * $0.01 \leq p < 0.05$, ** $0.001 \leq p < 0.01$, *** $0.0001 \leq p < 0.001$, **** $p < 0.0001$

DMD muscles ($1,325,645 \mu\text{m}^2 \pm 197,782$; Fig. 3F). Spearman's correlation analysis was also performed between the EBD-positive CSA and muscle fatigue outcomes in all groups combined. Significant negative correlation coefficients were found for both MCT after TMR ($r = -0.7$; Fig. 3G) and muscle fatigue ratio ($r = -0.4$; Fig. 3H), supporting that the decrease of damaged myofibers correlated with the amelioration of muscle fatigue tolerance of dystrophin supplemented-DMD muscles after cell transplantation.

Furthermore, the percentage of dystrophin and EBD double-positive myofibers ($0.02\% \pm 0.02$ of total dystrophin-positive fibers) confirmed that almost no dystrophin-supplemented myofiber was damaged after TMR (Fig. 3I), supporting that dystrophin protein has a protective role against myofiber damage created by TMR muscle fatigue. To confirm the conclusions in the even longer term, we performed the histological analysis of muscle damage using the EBD marker again in 33-wk mice (Fig. S3A). Likewise, the significant damage induced by TMR on DMD muscles compared to WT muscles tended to decrease in dystrophin supplemented-DMD muscles (Fig. S3B). The quasi-absence of dystrophin and EBD double-positive myofibers in the dystrophin-supplemented DMD muscles confirmed as well their stronger resistance against TMR-induced muscle damage even in 33-wk mice (Fig. S3C). Nevertheless, although previous muscle function evaluation in 21-wk mice revealed full recovery of muscle fatigue ratio after dystrophin supplementation (Fig. 1E), EBD-positive CSA still showed a significant difference between dystrophin supplemented-DMD muscles ($625,619 \mu\text{m}^2 \pm 110,484$) and WT muscles ($10,192 \mu\text{m}^2 \pm 4681$; Fig. 3F). These results indicate that a reduction in muscle damage alone cannot explain the full amelioration of muscle fatigue tolerance after dystrophin supplementation in DMD muscles.

DMD muscle fatigue amelioration after dystrophin supplementation, explained by a preferential regeneration of oxidative myofibers after cell transplantation

To further investigate the characteristics of the amelioration of DMD muscle fatigue tolerance after dystrophin supplementation, the myofiber types were studied in cross-sectional muscle tissue samples using immunohistochemistry. Firstly, myosin heavy chains type I (MHC-I) positive CSA was comparable in sedentary mice and in mice after TMR for both WT ($276,791 \mu\text{m}^2 \pm 31,452$ and $233,709 \mu\text{m}^2 \pm 55,753$, respectively; Fig. S4A) and DMD ($575,048 \mu\text{m}^2 \pm 98,517$ and $525,082 \mu\text{m}^2 \pm 40,727$, respectively) genotypes (Fig. S4B). The same applied to myosin heavy chain type IIA (MHC-IIA)-positive CSA (Fig. S4C, D). This confirmed that the myofiber

type had no relevance to the TMR. Of note, MHC-I positive CSA was significantly increased in dystrophin supplemented-DMD muscles ($1,473,036 \mu\text{m}^2 \pm 134,127$) compared to untreated DMD ($525,082 \mu\text{m}^2 \pm 40,727$) and WT ($233,709 \mu\text{m}^2 \pm 55,753$) muscles (Fig. 4A). As for type IIA fibers, the disease phenotype of preferential degeneration of fast fibers [44] was correctly reflected as MHC-IIA positive CSA in untreated DMD ($1,398,446 \mu\text{m}^2 \pm 153,213$) was significantly lower than in WT muscles ($2,177,655 \mu\text{m}^2 \pm 185,167$). In comparison, the phenotype was ameliorated after cell transplantation as MHC-IIA positive CSA in dystrophin supplemented-DMD muscles ($2,429,107 \mu\text{m}^2 \pm 148,435$) significantly regained WT levels (Fig. 4B). This particular balance between myofibers formed by MHC-I and MHC-IIA in DMD muscles after dystrophin supplementation was verified to remain the same in older, 33-wk mice (Fig. S4E, F). Observation of cross-sectional samples stained with an anti-myosin heavy chain type IIB (MHC-IIB) antibody qualitatively confirmed that myofibers negative for MHC-I and MHC-IIA were likely mouse type IIB fibers (Fig. S4G). These results suggested that dystrophin supplemented-DMD fibers were preferentially type I or type IIA in transplanted DMD muscles. To confirm this hypothesis, dystrophin- and MHC-I/IIA double-positive fibers were analyzed. $49.9\% \pm 4.3$ of dystrophin-supplemented DMD fibers were positive for MHC-I, and $35.5\% \pm 1.9$ were positive for MHC-IIA (Fig. 4C, D). As these two types of myosin chains are known to form oxidative type fibers [45, 46], these results indicated that an average of 85.4% of dystrophin-supplemented DMD myofibers preferentially used oxidative metabolism after cell transplantation, and the same experiments reconducted with 33-wk mice confirmed a percentage of 82.2% (Fig. S4H). Furthermore, as some reports have described type I myofibers as more resistant to damage than other fiber types [47], EBD and MHC-I double-positive fiber analyses were undertaken. Less than $0.4\% \pm 0.2$ of MHC-I positive fibers were EBD-positive in untreated DMD muscles after TMR, pointing out that type I fibers were indeed likely to manifest resistance toward muscle damage created by TMR muscle fatigue (Fig. 4E). Finally, the same analysis conducted in dystrophin-supplemented DMD muscles revealed a similar phenomenon at 21 (Fig. 4F) to that at 33 weeks of age (Fig. S4I) with almost no fiber, being concurrently positive for dystrophin, MHC-I, and EBD. These results attested that the vast majority of newly formed dystrophin-supplemented DMD fibers after cell transplantation were both oxidative and damage-resistant, and remained so over time.

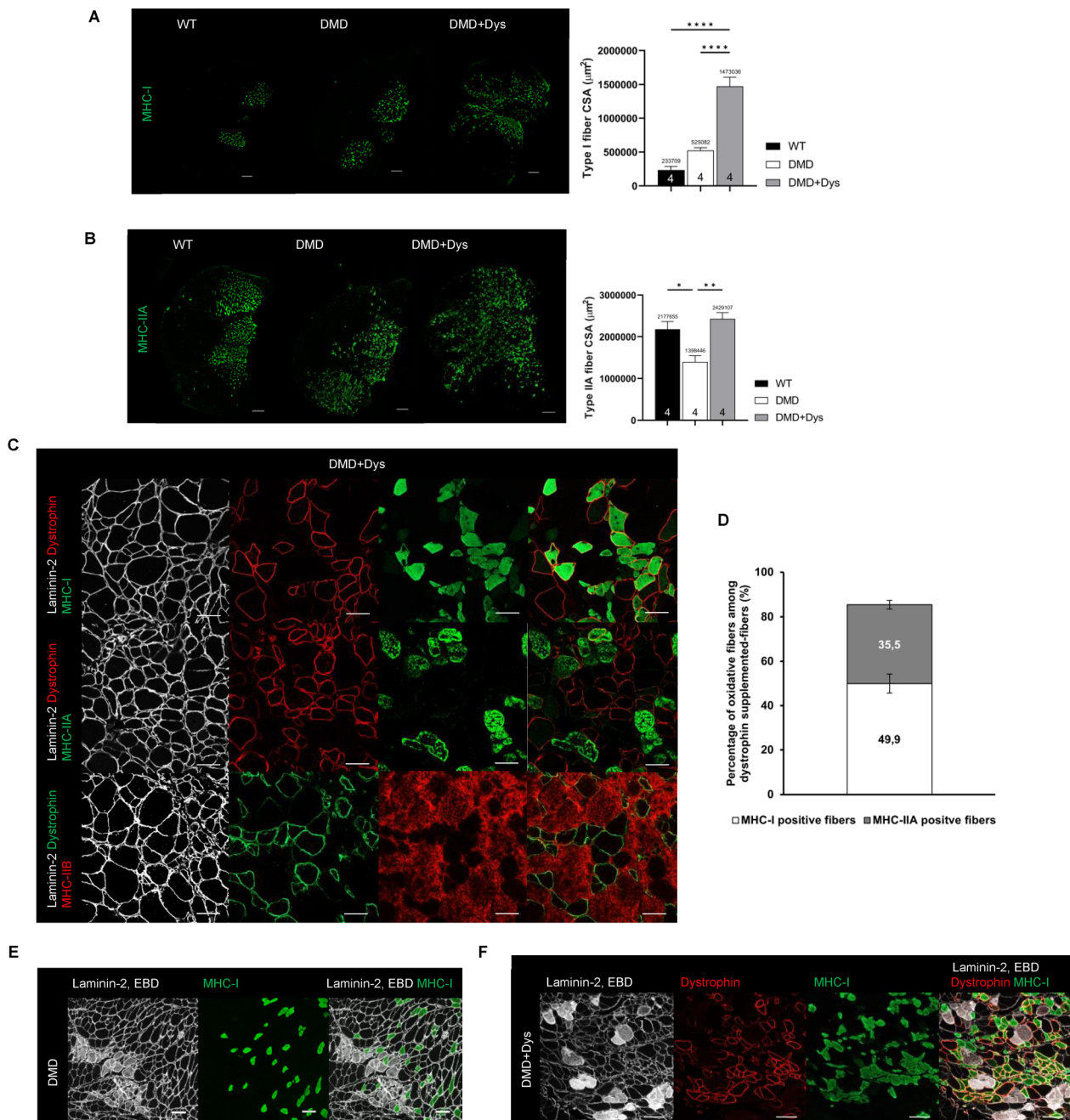


Fig. 4 Preferential regeneration of oxidative myofibers in DMD muscles after cell transplantation. **A** Sectional immunostaining images of whole gastrocnemius of 21-weeks old (wo) wild type (WT), untreated DMD (DMD) and dystrophin supplemented-DMD (DMD +Dys) mice collected after of treadmill running (TMR) assessment. Myosin heavy chains type I (MHC-I; green) were stained to evaluate the proportion of type I fibers in mouse gastrocnemius muscles. Scale bars: 500 μm . Quantitative graph shows type I fiber cross-sectional area (CSA). $n=4$. **B** Sectional immunostaining images of whole gastrocnemius of 21-wo WT, DMD and DMD +Dys mice collected after TMR assessment. Myosin heavy chains type IIA (MHC-IIA; green) were stained to evaluate the proportion of type IIA fibers in mouse gastrocnemius muscles. Scale bars: 500 μm . Quantitative graph shows type IIA fiber CSA. $n=4$. **C** Sectional immunostaining images of gastrocnemius muscles of 21-wo DMD +Dys mice collected after TMR assessment. Dystrophin and laminin-2 were stained with myosin heavy chains types I/IIA/IIB to evaluate the predominant fiber type among dystrophin-supplemented DMD fibers after cell transplantation. Scale bars: 50 μm . **D** Quantitative analysis of myosin heavy chain types showing predominance of oxidative fibers in dystrophin-supplemented DMD fibers after cell transplantation. $n=4$. **E** Sectional immunostaining images of gastrocnemius of 21-wo DMD mice collected after TMR assessment. No fiber were both positive for EBD (CSA stained in white) and MHC-I (green). Scale bars: 100 μm . **F** Sectional immunostaining images of gastrocnemius of 21-wo DMD +Dys mice collected after TMR assessment. No fiber were concurrently positive for dystrophin (red), EBD (CSA stained in white) and MHC-I (green). Scale bars: 100 μm . Data are shown as mean \pm SEM. * $0.01 \leq p < 0.05$, ** $0.001 \leq p < 0.01$, **** $p < 0.0001$

DMD muscle fatigue amelioration after dystrophin supplementation, ascribed to higher mitochondrial activity in dystrophin supplemented-DMD muscles

Myofibers are characterized by different metabolic properties. Glycolytic fibers primarily use anaerobic glycolysis as an ATP source and generate quick and strong contractions but are easily fatigable [45, 48]. In contrast, oxidative fibers create ATP from oxygen and glucose through aerobic respiration, have a slower speed and shortening tension, but are highly resistant to fatigue [45, 48]. Based on this knowledge, animal experiments were conducted to confirm the changes in metabolic functions caused by dystrophin supplementation in the DMD muscle. Thus, a novel GO-ATeam2 transgenic (ATPtg) *Dmd*-null/NSG mouse model that allows real-time in vivo ATP level monitoring was generated for the first time (Fig. S5A). Using these APTtg DMD mice, live ATP imaging was conducted so that 10 images per second of 20-week mouse gastrocnemius muscles were taken while undergoing muscle fatigue created by electrically stimulated repeated isometric contractions (RIC) at 40% of maximal contraction strength (Fig. 5A). Qualitative analysis of successive images showed lower ATP levels in APTtg DMD mouse muscles than in APTtg WT mice, which displayed high ATP levels in their entire gastrocnemius muscles (Fig. 5B). Compared to untreated APTtg DMD mice, dystrophin supplemented-ATPtg DMD muscles exhibited an increased ATP activity despite not as remarkable as that in APTtg WT mice. Then, averages of 10 images were calculated from quantitative data to study the relative ATP level time-course evolution during repeated contractions (Fig. 5C). The APTtg WT mouse curve showed a decrease in ATP level at the beginning of the contraction session, followed by an increase that widely surpassed the starting level until the cessation of contractions.

Conversely, the APTtg DMD mouse curve only presented a slow and mild increase during all repeated contractions. As for the dystrophin supplemented-ATPtg DMD mice curve, even if the ATP starting decrease was greater than in APTtg WT mice muscles, the ATP level increase afterward was much more noticeable than that of APTtg DMD mice (Fig. 5C). ATP level after the stop of repeated contractions was confirmed lower in APTtg DMD muscles (3.11 ± 0.24) compared to APTtg WT (3.99 ± 0.25 ; significant statistical Student's t-test result between the two groups; Fig. 5D). Of note, a higher level trend was observed in dystrophin supplemented-ATPtg DMD muscles (3.38 ± 0.26) compared to untreated APTtg DMD muscles (3.11 ± 0.24), even though statistical significance could not be proven (by one-way ANOVA in the three studied groups) likely due to the reduced sample size (Fig. 5D). The analysis of the ATP level ratio before and after the contraction session revealed similar results (Fig. 5E). Moreover, functional results were analyzed to confirm that the muscular work induced by RIC had the same functional effects as the previously tested TMR. Despite the absence of statistical significance, APTtg DMD mice muscle fatigue ratio outcome was predictably reduced compared to both APTtg WT and dystrophin supplemented-ATPtg DMD mice muscles (Fig. S5B).

Oxidative phosphorylation (OXPHOS) activity in skeletal muscle mitochondria, known to produce ATP, was further investigated after TMR by western blot analysis of the electron transport chain complex subunits (Figs. 5F, S5C, D, E). The abundance of mitochondrial OXPHOS complexes II, III, IV, and V was lower in DMD muscles than in WT muscles. More importantly, an increase of these complexes was detected in dystrophin supplemented-DMD muscles compared to untreated DMD muscles (Figs. 5F, S5C, D, E), suggesting higher

(See figure on next page.)

Fig. 5 High mitochondrial activity in dystrophin supplemented-DMD muscles after cell transplantation. **A** Schematic representation of in vivo live ATP imaging in 20-weeks old (wo) GO-ATeam2 transgenic wild type (ATPtg WT), untreated DMD (ATPtg DMD) and dystrophin supplemented-DMD (ATPtg DMD + Dys) mouse gastrocnemius during fatigue induced by repeated isometric contractions (RIC). **B** ATP images of 20-week APTtg WT, DMD and DMD + Dys mouse gastrocnemius during RIC, showing low (blue) to high (red) ATP level. **C** Time-course ATP relative level (average/second) in 20-week APTtg WT, DMD and DMD + Dys mouse gastrocnemius during RIC. $n=8$ (ATPtg WT), $n=5$ (ATPtg DMD), $n=5$ (ATPtg DMD + Dys). **D** ATP level of 20-week APTtg WT, DMD and DMD + Dys mouse gastrocnemius assessed after RIC. Sample sizes: cf. **C**. **E** ATP level ratio of 20-week APTtg WT, DMD and DMD + Dys mouse gastrocnemius before and after RIC. Sample sizes: cf. **C**. **F** Cropped western blot of mitochondrial electron transport chain complexes and GAPDH in 21-week wild type (WT), untreated DMD (DMD) and dystrophin supplemented-DMD (DMD + Dys) mouse gastrocnemius collected after treadmill running (TMR) assessment. From top to bottom: ATP synthase subunit-alpha of complex-V; cytochrome b-c1 complex subunit-2 of complex-III; cytochrome c oxidase subunit-1 of complex-IV; GAPDH; succinate dehydrogenase subunit-B of complex-II. The full-length blots and Coomassie brilliant blue-stained blot used as control are presented in Supplementary Fig. 5. $n=4$. **G** Sectional electron microscopy images of 27-week WT, DMD and DMD + Dys mouse gastrocnemius collected after TMR assessment. Image sizes: $22.3 \mu\text{m} \times 16.7 \mu\text{m}$ (upper panel), $5.6 \mu\text{m} \times 4.2 \mu\text{m}$ (lower panel). **H** Sectional electron microscopy images of 27-week WT, DMD and DMD + Dys mouse gastrocnemius collected after TMR assessment. Image sizes: $1.9 \mu\text{m} \times 1.4 \mu\text{m}$. **I** Sectional images of 21-week DMD + Dys mouse gastrocnemius collected after TMR assessment. Dystrophin (red) and NADH-TR (purple-blue) were stained to compare mitochondrial activity between dystrophin-positive/negative fibers. Scale bars: $50 \mu\text{m}$. Quantitative graphs show range of intensity (0 black; 256 absence of signal) and staining intensity. $n=6$. Data are shown as mean \pm SEM. * $0.01 \leq p < 0.05$

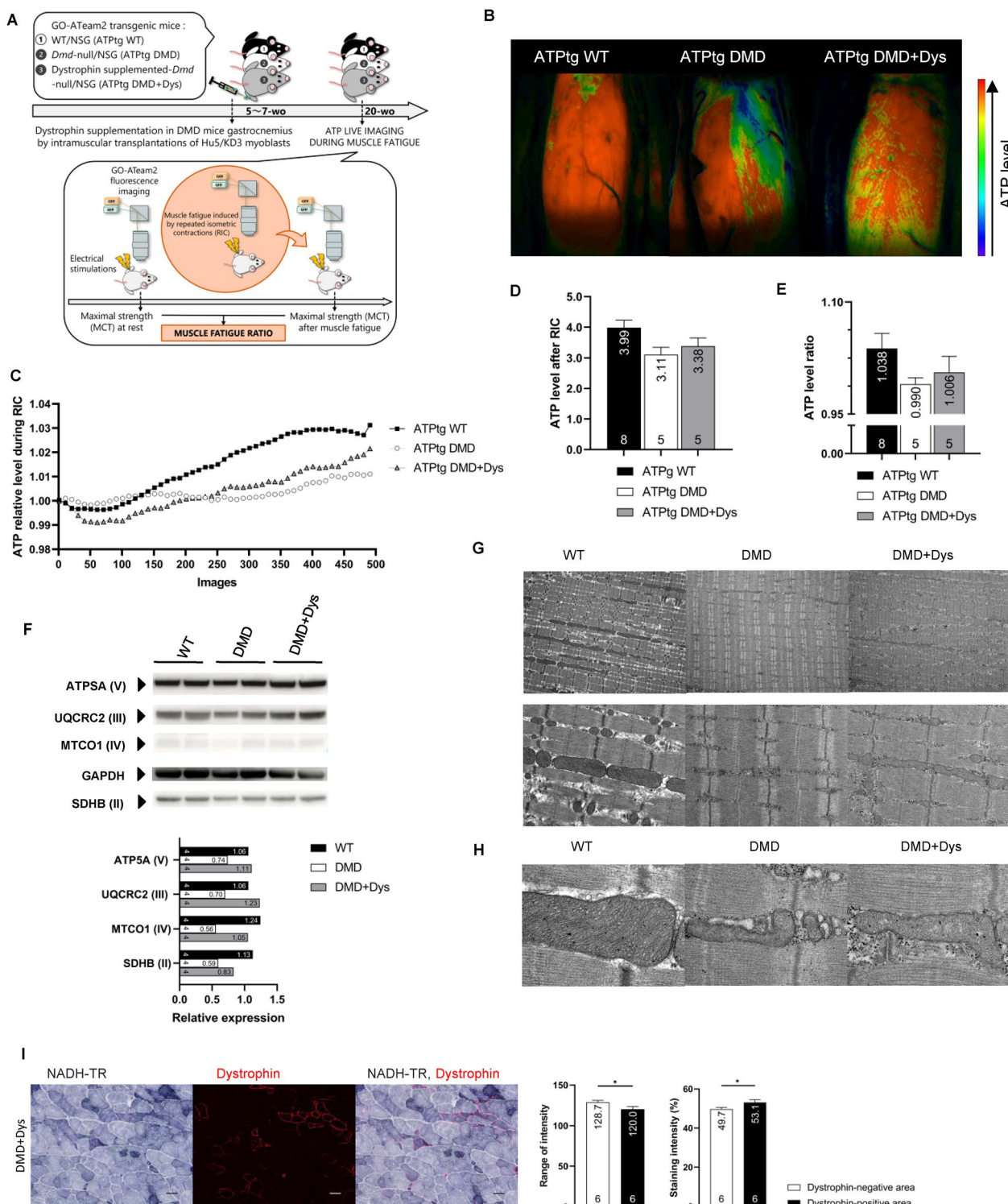


Fig. 5 (See legend on previous page.)

mitochondrial activity in DMD skeletal muscles after dystrophin supplementation. Further study of mitochondrial organelles in 27-wo mice muscle tissue samples collected

immediately after TMR evaluation was performed using TEM. Longitudinally sectioned-WT muscle samples contained numerous normally-shaped mitochondria

between myofibers sarcomeres (Fig. 5G), with a high density of cristae in their inner membrane (Fig. 5H). In untreated DMD muscle samples, the mitochondria were fewer, smaller, and sparser, while the mitochondrial internal structure appeared less dense and complex, with very few cristae compared to WT mitochondria (Fig. 5G, H). Dystrophin supplemented-DMD muscles contained more mitochondria than untreated DMD muscles, and in some parts of observed muscle samples, they visually resembled WT ones (Fig. 5G, H). These results indicate a reduction in mitochondrial impairment in the number and structure of DMD muscles following dystrophin supplementation via cell transplantation. To confirm these data, nicotinamide adenine dinucleotide-tetrazolium reductase (NADH-TR) was stained in transplanted DMD mice muscle samples, and the range of intensity was compared between dystrophin-positive and -negative fibers within the same muscle sample sections (Figs. 5I, S5F). For each sample, average brightness was found to be significantly higher in dystrophin-negative fibers (128.7 ± 2.44 average range of intensity) compared to dystrophin supplemented-DMD fibers (120.0 ± 3.55 average range of intensity; Figs. 5I, S5F). The NADH-TR reaction studied in the muscles of 33-wk mice was conclusive as well and validated those findings in the even longer term (Figs. S5G, H). Consistent with myofiber-type results, these data further supported that dystrophin supplemented-DMD fibers presented higher mitochondrial oxidative activity than untreated DMD fibers.

Discussion

In this study, we established a novel method for the accurate evaluation of DMD mouse motor function, overcoming the different issues of previously reported methods. Notably, its application successfully demonstrated the beneficial effects of cell therapy-mediated dystrophin supplementation on DMD muscle fatigue tolerance. Investigations into the molecular mechanisms explained this functional amelioration by the preferential regeneration of damage-resistant and oxidative myofibers with high mitochondrial activity after cell transplantation.

First, our new functional evaluation method properly reflected DMD motor function deficiencies compared to the WT mouse model over a long period. Our large sample size permitted the validation of these functional results with high statistical significance. Different methods, with both advantages and disadvantages, have been reported regarding the assessment of cell therapy efficiency in DMD motor function. Muscle tension measurements have been performed *ex vivo* (after animal sacrifice, muscle contractile properties are evaluated outside its physiological environment using *in vitro* systems) [25, 26, 28, 31, 34, 49] or *in situ* (under animal anesthesia,

one tendon remains attached to the organism, while the other is exposed, sectioned, and attached to a force transducer) [32, 33]. Although these methods are specific to the targeted muscle, they only enable a one-time assessment, and the need to harvest all or part of the muscle renders them far from any possible clinical application in patients with DMD. Additionally, an *in vivo* method using transcutaneous electrical stimulation to generate tetanic muscle contractions under anesthesia has been reported [29]. This method overcomes the previously described disadvantages and allows multiple time-point evaluations of the same individual. However, our experiments indicated that the MCT values resulting from transcutaneous electrical stimulations of the gastrocnemius could not accurately reflect the therapeutic effect of cell transplantation therapy on DMD muscles. On another note, some reported methods show more functionality than electrical stimulation and are suitable for time-course evaluation; however, they remain disputable. For instance, the accuracy of the grip strength test [34, 49, 50] has been debated because of operator bias [51]. The test constrains the assessment of several limbs together and in their global flexion movement; moreover, the reproducibility of a stable evaluation position is limited. The same applies to the wire hang test [50] which is not muscle-specific, as it recruits whole animal muscles as well as balance abilities to resist hanging fatigue. As for exhaustion tests using wheels or treadmills [28, 52], although they appropriately reflect DMD functional ambulatory needs in daily living, the evaluation until exhaustion cannot be considered clinically. In addition, running tests have the disadvantage of taking the whole body into account, especially the cardiorespiratory system [53] which deteriorates in DMD [54]. Considering each existing method, we aimed to combine their advantages to create a novel and relevant evaluation protocol for DMD motor functions. Thus, in our approach, muscle fatigue was created in live animals using a treadmill in a functional and clinically applicable way that could be replaced by a walking test usually used with patients, such as the six-minute walk test [55]. Additionally, *in vivo*, transcutaneous electrical stimulations were used to reflect strength decline, so that muscle specificity and functioning environment were maintained and that repeated assessments in the same individual were feasible to detect functional changes over time. Another advantage was the establishment of the first functional evaluation method for the *Dmd*-null/NSG mouse model, where most studies used an *mdx* mouse model, even though its dystrophic features are minimal during the 0–2 weeks and 3–6 weeks phases, with severe phenotypes only occurring at around 15 months of age [56]. Moreover, due to a nonsense mutation in the *Dmd* gene, *mdx* muscles

do not completely lack dystrophin protein, making the distinction between the effects of endogenous or supplemented dystrophin in cell transplantation studies difficult [57]. Finally, our method with the *Dmd*-null/NSG mouse model enabled the long-term evaluation of cell therapy efficiency, whereas most studies only focused on mice of a few weeks of age, which constitutes an essential criterion considering future clinical application needs.

In addition to overcoming issues of the reported methods, the application of our novel method reliably demonstrated significant and long-term amelioration of muscle fatigue tolerance after cell therapy-mediated dystrophin supplementation in DMD muscles. Among the animal studies that investigated dystrophic mouse muscle function after cell therapy, a few reported improvements in fatigue resistance. Earlier tests consist of *ex vivo* tests [31, 49], *in situ* tests [32, 33] and treadmill exhaustion tests [28, 52] which present the above-described numerous disadvantages. Therefore, for the first time, the present *in vivo* study could validate the findings with high significance without implementing invasive methods and strictly maintaining the assessed muscle in its molecular physiological environment. Furthermore, our study confirmed that cell therapy-mediated dystrophin supplementation was responsible for the full recovery of DMD muscle fatigue tolerance at 21 weeks of age, as no statistical difference was observed between WT and dystrophin supplemented-DMD groups. In addition, the literature provides reviews exploring the effects of TMR on DMD mouse performance [58, 59]. However, the intensity (duration, speed, slope), acclimatization (acceleration, pre-training), and frequency of running sessions differed between studies, and we could not find gold-standard protocols or investigations on *Dmd*-null/NSG mouse models. As no direct comparison was possible between our results and those in the literature, additional experiments were conducted to compare the muscle fatigue outcomes between sedentary mice and mice that had undergone several tests. Thus, we successfully confirmed that our treadmill evaluation method itself did not improve mouse performance and, consequently, that cell therapy-mediated dystrophin supplementation directly ameliorated DMD muscle fatigue tolerance. Finally, the functional results of 33-week mice supported that this functional amelioration is likely to persist over time and in the very long term, even though the difficulty in keeping our DMD mouse model alive limited our possibilities to statistically confirm that hypothesis. As the age-related muscle fatigue tolerance reduction also could be observed in the WT group, the absence of significant results at 33 weeks of age might not reflect a reduced treatment efficacy but could be explained by the unavoidable use of immunodeficient mouse models for

transplantation studies using human cells. The diminished muscle functions observed in WT/NSG mice would be a consequence of the diabetic background as these animals are non-obese diabetic (NOD) mice.

We investigated several possible mechanisms involved in the amelioration of DMD muscle fatigue tolerance following cell therapy-mediated dystrophin supplementation. Even though mouse muscles, including gastrocnemius, are highly composed of fast-twitch glycolytic fibers, contrary to human muscles [60], we have found that 85.4% of dystrophin-supplemented mice myofibers newly regenerated after cell transplantation were oxidative type. The metabolism of oxidative fibers (composed of type I slow oxidative and type IIA fast oxidative fibers) primarily involves aerobic respiration instead of glycolysis, which induces slow contractions but provides high resistance to fatigue [45]. Thus, the full amelioration of DMD muscle fatigue observed in our study was ascribed to the preferential regeneration of dystrophin-positive oxidative myofibers after cell transplantation. These results are in accordance with a previous report that described the high expression of type I fibers after the transplantation of mouse myogenic progenitors in both dystrophic and healthy mouse skeletal muscles [61]. Furthermore, we confirmed for the first time that the transplantation of human cells expressing dystrophin ameliorates DMD motor functions through the preferentially directed regeneration of dystrophin-positive oxidative myofibers. First, we hypothesized that dystrophin protein could somehow protect myofibers from muscle damage generated by the TMR load. Looking at our study results, several points were in favor of this statement: WT fibers were not damaged after TMR contrary to DMD fibers, damaged muscle area was reduced in dystrophin supplemented-DMD muscles compared to untreated DMD control, and almost none of dystrophin-supplemented DMD fibers were damaged after TMR. Second, we hypothesized that the reduced damage after muscle fatigue loading could also originate from the high proportion of slow fibers found in the DMD muscles after dystrophin supplementation. Indeed, slow fibers are reported to be more resistant than other fiber types and, thus, are less easily damaged by muscle contraction exercises [47]. In dystrophic muscles, the myofiber-type balance is disturbed [46] due to the preferential degeneration of fast-twitch myofibers, such that slow degeneration-resistant fibers are the most spared [44]. This was verified in our DMD samples, and none of the type I fibers were damaged after TMR. Of note, we found no dystrophin-supplemented slow oxidative fiber that was damaged by TMR in DMD muscle after cell transplantation, which was consistent with one or the other of the previously two stated hypotheses.

Furthermore, oxidative fibers contain large numbers of mitochondria with a dense cristae ultrastructure to produce ATP via a unique and self-sufficient synthesis mechanism that involves mitochondrial oxidative phosphorylation [45, 62]. As expected, we also observed enhanced mitochondrial related-outcomes in dystrophin supplemented-DMD muscles compared to untreated DMD samples: more numerous mitochondrial organelles, ultrastructure with more densely packed cristae, more abundant electron transport chain complexes, and significantly higher NADH-TR activity. So far, *in vitro* experiments on isolated mitochondria have widely assumed that low ATP synthesis is a result of mitochondrial dysfunction in DMD [63, 64]. Noninvasive spectroscopic methods have also emerged in the last decade for *in vivo* assessment in animal models of DMD [63, 65, 66]. Here, the creation of a novel GO-Ateam2 transgenic DMD mouse model goes further, leading to the first *in vivo*, live, and direct demonstration of the ATP level-impaired phenotype in DMD skeletal muscles, especially during real-time muscle exercise. Moreover, we have observed trends of amelioration in ATP levels in dystrophin supplemented-DMD muscles. Although the limited sample size did not work in favor of statistical significance, these results were consistent in all tested types of analyses: qualitative analysis of ATP dynamics successive images, real-time quantification of ATP relative level during RIC, and calculation of the ATP level decrease ratio before and after the contraction session. Results suggested that as WT muscles, supplemented DMD muscles first displayed a decrease of ATP due to the start of contraction activity but had an increased ability to adapt and raise their ATP level in response to that demand compared to DMD muscles. Indeed, it has been reported that an imbalance in ATP dynamics in DMD may diminish muscle tolerance to repeated contractions and exercise [67]. Because ATP measurements were conducted by imaging the surface of gastrocnemius muscles, it is probable that we detected enhanced ATP levels in the newly regenerated dystrophin-positive type IIA fibers that were present near the muscle surface, as shown in histological immunostaining images. Furthermore, we have confirmed that even within the same transplanted DMD muscle sample, mitochondrial activity reflected by NADH-TR activity was significantly higher in dystrophin-positive fibers compared to dystrophin-negative fibers, validating that dystrophin supplemented-DMD fibers were undoubtedly at the origin of muscle fatigue tolerance improvement. The similar results obtained after histological analysis performed at several time-points (i.e., 21 and 33 weeks of age) demonstrated the long-term validity of these findings. In addition, as only 10% supplementation could fully ameliorate DMD muscle fatigue

tolerance function, we prospected that dystrophin-positive fibers displaying higher mitochondrial activity could influence the surrounding fibers, increasing the global mitochondrial dynamics and the whole muscle tolerance toward muscle fatigue via some still unclear molecular mechanisms. It would be relevant to further investigate these mechanisms in future studies.

Regarding the above-mentioned dystrophin supplementation efficiency, we confirmed dystrophin protein expression in the skeletal muscles of our DMD mouse model after conducting multiple local transplantations of healthy human myoblasts, which was the most effective way to obtain a large number of dystrophin-expressing cells and supplement DMD muscles. Extensive research using different approaches for supplementation investigated the minimum number of dystrophin-supplemented fibers required to detect an amelioration in DMD function. Depending on the research groups, at least 15 to 20% dystrophin-supplemented DMD fibers were found necessary in mouse experiments [68–71]. Those thresholds represent key values from a clinical application perspective and future transplant experiments in human DMD patients as, so far, no clinical case has been specifically published concerning the correlation between dystrophin levels and DMD motor function outcome severity. We found that 10% of dystrophin-positive fibers counted in transplanted DMD muscles were sufficient to ameliorate the two types of DMD muscle functions, indicating higher efficiency with a lower dystrophin supplementation rate compared to that reported in previous studies. Indeed, we provided evidence that cell therapy-mediated dystrophin supplementation was not only efficient in DMD muscle fatigue tolerance but could also prevent severe DMD muscle weakness, as indicated by the ROC curve analysis results. A clinical study of Becker muscular dystrophy (BMD) validated the determinant limit of 10% dystrophin-expressing myofibers for BMD muscle function symptom onset and severity, *inter alia*, in the case of the maximal voluntary isometric contraction of the patients [72]. Therefore, 10% dystrophin supplementation rate could be sufficient also in human patients with DMD at least to prevent severe cases, enabling such patients to reach a BMD phenotype in terms of muscle functions. Interestingly, the functional evaluation of MCT values in our study did not detect any significant effect of dystrophin supplementation on the maximal strength function of DMD mice. Consistently with our metabolic studies, this must put forward the differences between anaerobic (as maximal contraction) and aerobic (as running) muscular exercises. A significant correlation was yet revealed between the number of dystrophin-supplemented DMD fibers and MCT at rest. This correlation was even stronger when analyzing samples from the

oldest 33-week mice. A gradual increase in necrosis has been reported in the myofibers of DMD patients with aging, along with decreasing regenerative abilities due to the senescence of satellite cells [73]. Thus, progressive impairment of the surrounding non-supplemented DMD fibers with aging may have provided a stronger impact on the remaining dystrophin supplemented-DMD fibers. We first speculated that our study's functional results were limited by the absence of highly dystrophin supplemented-DMD samples. However, regenerating myofibers remained smaller than WT myofibers after transplantation. As the tension resulting from myofiber contraction is known to be proportional to its diameter [43], which is related to the number of recruitable neuromuscular junctions in the fiber, we concluded that even a higher number of dystrophin supplemented-DMD fibers might not be sufficient to regain as much strength as in WT mice, as long as they remain smaller. Therefore, we are currently investigating whether the therapeutic effect of cell therapy can be maximized by adding complementary interventions, such as muscle training exercises, to promote the regeneration of more hypertrophied dystrophin supplemented-DMD myofibers after cell transplantation.

Last but not least, the present literature in the DMD field left no doubt on our ability to supplement the lacking dystrophin protein in DMD muscles, or even to improve resulting dystrophic histology or systemic features. However, the novelty of this study could be highlighted as we are now able to affirm with certainty that cell therapy efficiently improves DMD motor functions. This result was achievable by the successful establishment of accurate, reproducible, and reliable novel assessment methods in vivo that overcame the remaining technical difficulties and limitations of previous studies. Of note, we discovered that muscle fatigue tolerance is a relevant outcome to study cell therapy efficacy in DMD muscles. Moreover, our long-term study results are significant in prospects of clinical trials as the low threshold of 10% dystrophin supplementation rate was durably efficient to affect DMD motor functions. More than sole treatment efficacy, the regenerating oxidative myofiber increase after cell transplantation deepens our knowledge on the molecular mechanisms that are still elusive and lead to DMD pathogenesis, providing the basis for establishing future therapeutic approaches for DMD.

Conclusions

Through a cell transplantation study in *Dmd*-null/NSG mouse model, we established novel evaluation methods that successfully demonstrated the long-term efficacy of cell therapy-mediated dystrophin supplementation on DMD motor functions. Thus, even low dystrophin

supplementation rates prevented severe muscular weakness and significantly, fully, and durably ameliorated muscle fatigue tolerance in DMD muscles. The latter functional improvement was explained by the preferential regeneration of dystrophin-positive myofibers with protective properties against muscle damage and oxidative metabolic functioning with high mitochondrial activity after cell transplantation. Therefore, this research brought novel, valuable findings toward clinical application as reliable measurement methods and validation of the long-term efficiency of cell therapy on DMD motor functions.

Abbreviations

ADL	Activities of daily living
AMED	Japan Agency for Medical Research and Development
ANOVA	Analysis of variance
AP	Alkaline phosphatase
ARRIVE	Animal research: reporting of in vivo experiments
ATP	Adenosine triphosphate
ATPtg	GO-ATeam2 transgenic
AUC	Area under the curve
BMD	Becker muscular dystrophy
CBB	Coomassie brilliant blue
CSA	Cross-sectional area
DAPC	Dystrophin-associated protein complex
DAPI	4',6-Diamidino-2-phenylindole, dihydrochloride
DMD	Duchenne muscular dystrophy
DMEM	Dulbecco's modified eagle medium
D-PBS	Dulbecco's phosphate-buffered saline
EBD	Evans blue dye
FRET	Förster resonance energy transfer
GAPDH	Glyceraldehyde 3-phosphate dehydrogenase
IHC	Immunohistochemistry Laminin-2 Laminin protein subunit alpha 2
MCT	Maximal isometric contraction torque
MCT/BW	Maximal isometric contraction torque normalized to mouse body weight
MHC-I	Myosin heavy chain type I
MHC-IIA	Myosin heavy chain type IIA
MHC-IIB	Myosin heavy chain type IIB
NADH-TR	Nicotinamide adenine dinucleotide-tetrazolium reductase
NGS	Normal goat serum
NOD	Non-obese diabetic
N.S.	Not significant
NSAA	NorthStar Ambulatory Assessment
NSG	NOD.Cg-Prkdc ^{scid} Il2rg ^{tm1Wjl} /SzJ
OXPHOS	Oxidative phosphorylation
<i>p</i>	<i>p</i> -value
PB	Phosphate buffer
PBS-T	Dulbecco's phosphate-buffered saline supplemented by Triton X-100
PO	Propylene oxide
<i>r</i>	Spearman's rank correlation coefficient
RIC	Repeated isometric contractions
RIPA	Radioimmunoprecipitation assay
ROC	Receiver operating characteristic
SD	Standard deviation
SEM	Standard error of the mean
TBS	Tris-buffered saline
TBS-T	Tris-buffered saline supplemented by Triton X-100
TEM	Transmission electron microscopy
TMR	Treadmill running
WB	Western blot
Wo	Week-old
WT	Wild type

Supplementary Information

The online version contains supplementary material available at <https://doi.org/10.1186/s13287-024-03922-x>.

Supplementary Material 1.

Acknowledgements

We thank N. Hashimoto for providing the Hu5/KD3 cell line, A. Tanaka for conducting *Dmd*-null/NSG mice in vitro fertilization, T. Yoshida for advice on analyzing electron microscopy images, H. Takenaka for advice on statistical analysis, R. Ikeda, M. Tanaka, R. Kawabe, and N. Ooka for technical support during cell culture and/or mouse functional assessments, and M. Zhao for technical support during western blot experiments. The authors declare that artificial intelligence is not used in this study.

Author contributions

N.T.-N. and H.S. are the lead contacts in this study. C.K.B.Y., H.S., and N.T.-N. were responsible for the study conception, experimental design, data interpretation, manuscript preparation, and final validation. C.K.B.Y. conducted most experiments. C.K.B.Y., N.T.-N., M.G., and M.M. performed the cell culture and mouse functional assessments. C.K.B.Y. and N.T.-N. performed the transplantation experiments. M.Y. generated the GO-Ateam2 transgenic mouse model and conceived the ATP imaging system. D.W. performed the ATP imaging experiments in the GO-Ateam2 transgenic DMD mouse model, and C.K.B.Y. and N.T.-N. performed the ATP image analysis. All the authors discussed the results. C.K.B.Y., N.T.-N., T.A., and H.S. wrote, reviewed, and edited the manuscript. T.A. and H.S. were committed to project administration. H.S., N.T.-N., and M.Y. acquired funding.

Funding

This work was mainly supported by a grant from the Core Center for iPS Cell Research (JP13bm0104001 to H.S.), which is a program in the Research Center Network for Realization of Regenerative Medicine provided by the Japan Agency for Medical Research and Development (AMED). This work was partly supported by a grant from the Core Center for Regenerative Medicine and Cell and Gene Therapy (JP23bm1323001 to H.S.), which was part of the Acceleration Program of R&D and Implementation for Regenerative Medicine and Cell and Gene Therapy by AMED. This work was also partially supported by a Grant-in-Aid for JSPS Fellows (17J40184 to N.T.-N.), provided by the Japan Society for the Promotion of Science, and by a grant provided by the AMED (22ama121050j0002, 20ek0610017h0003, to M.Y.).

Availability of data and materials

The data generated and analyzed in the current study are available from the lead contact upon reasonable request.

Declarations

Ethics approval and consent to participate

All animal experiments were performed in compliance with the regulations of the Kyoto University Recombinant DNA Experiment Safety Committee and were approved by the Kyoto University Animal Experiment Committee ("Research on rehabilitation interventions to maximize the therapeutic effect of cell transplantation in a model of refractory muscle disease", No. 17-81, approved on March 17, 2017; "Experiments to elucidate the pathogenesis mechanisms of DMD mouse model by applying ATP visualization technology", No. 20-141, approved on October 7, 2020) and by the Committee of Experimental Animal Research of National Cerebral and Cardiovascular Center ("Studies on the dynamics of energy metabolism in mice and rats in vivo", 21053, 22029, 23018, approved on June 16, 2021). All animal models and experimental procedures conformed to the National Institutes of Health Guide for the Care and Use of Laboratory Animals. Generation of human immortalized myoblasts Hu5/KD3 was approved by the Ethics Committee of the National Center for Geriatrics and Gerontology ("Molecular and Cellular Biological Analysis of Tissue repair and Regeneration", No. 09-01, approved in October, 2009), and was conducted from the human primary myoblasts obtained by biopsy from a 44-year-old woman with informed consent at the Kanagawa Cancer Center Research Institute as described by Wada et al. [74].

The Hu5/KD3 cells were transferred to Kyoto University by Material Transfer Agreement (OUTBOUND QUICK-MATERIAL TRANSFER AGREEMENT, signed on February 7, 2013).

Consent for publication

Not applicable.

Competing interests

The authors declare that they have no competing interests.

Author details

¹Department of Clinical Application, Center for iPS Cell Research and Application, Kyoto University, 53 Kawahara-cho, Shogoin, Sakyo-ku, Kyoto 606-8507, Japan. ²Department of Advanced Physical Therapy, Human Health Sciences, Graduate School of Medicine, Kyoto University, 53 Kawahara-cho, Shogoin, Sakyo-ku, Kyoto 606-8507, Japan. ³Department of Rehabilitation Medicine, Graduate School of Medical Sciences, Nagoya City University, 1 Kawasumi, Mizuho-cho, Mizuho-ku, Nagoya 467-8601, Japan. ⁴Graduate School of Sport and Health Sciences, Osaka University of Health and Sport Sciences, 1-1 Asashirodai, Kumatori-cho, Sennan-gun, Osaka 590-0496, Japan. ⁵Department of Research Promotion and Management, National Cerebral and Cardiovascular Center, 6-1 Kishibe-Shimmachi, Suita, Osaka 564-8565, Japan.

Received: 18 December 2023 Accepted: 4 September 2024

Published online: 19 September 2024

References

- Duchenne G. Paraplegie hypertrophique de l'enfance de cause cerebrale. Paris: Bailliere et Fils; 1861.
- Crisafulli S, Sultana J, Fontana A, Salvo F, Messina S, Trifiro G. Global epidemiology of Duchenne muscular dystrophy: an updated systematic review and meta-analysis. *Orphanet J Rare Dis.* 2020;15:141.
- Markati T, Oskoui M, Farrar MA, Duong T, Goemans N, Servais L. Emerging therapies for Duchenne muscular dystrophy. *Lancet Neurol.* 2022;21:814–29.
- Mercuri E, Bönnemann CG, Muntoni F. Muscular dystrophies. *Lancet.* 2019;394:2025–38.
- Bladen CL, Salgado D, Monges S, Foncuberta ME, Kekou K, Kosma K, et al. The TREAT-NMD DMD global database: analysis of more than 7000 Duchenne muscular dystrophy mutations. *Hum Mutat.* 2015;36:395–402.
- Hoffman EP, Brown RH Jr, Kunkel LM. Dystrophin: the protein product of the Duchenne muscular dystrophy locus. *Cell.* 1987;51:919–28.
- Campbell KP, Kahl SD. Association of dystrophin and an integral membrane glycoprotein. *Nature.* 1989;338:259–62.
- Gao QQ, McNally EM. The dystrophin complex: structure, function, and implications for therapy. *Compr Physiol.* 2015;5:1223–39.
- Royuela M, Chazalotte D, Hugon G, Paniagua R, Guerlavais V, Fehrentz JA, et al. Formation of multiple complexes between beta-dystroglycan and dystrophin family products. *J Muscle Res Cell Motil.* 2003;24:387–97.
- Dubuisson N, Versele R, Planchon C, Selvais CM, Noel L, Abou-Samra M, et al. Histological methods to assess skeletal muscle degeneration and regeneration in Duchenne muscular dystrophy. *Int J Mol Sci.* 2022;23(24):16080.
- Ervasti JM. Dystrophin, its interactions with other proteins, and implications for muscular dystrophy. *Biochim Biophys Acta.* 2007;1772:108–17.
- Birnkranz DJ, Bushby K, Bann CM, Apkon SD, Blackwell A, Brumbaugh D, et al. Diagnosis and management of Duchenne muscular dystrophy, part 1: diagnosis, and neuromuscular, rehabilitation, endocrine, and gastrointestinal and nutritional management. *Lancet Neurol.* 2018;17:251–67.
- Patterson G, Conner H, Groneman M, Blavo C, Parmar MS. Duchenne muscular dystrophy: current treatment and emerging exon skipping and gene therapy approach. *Eur J Pharmacol.* 2023;947: 175675.
- Matthews E, Brassington R, Kuntzer T, Jichi F, Manzur AY. Corticosteroids for the treatment of Duchenne muscular dystrophy. *Cochrane Datab Syst Rev.* 2016;2016: CD003725.
- Ward LM, Hadjiyannakis S, McMillan HJ, Noritz G, Weber DR. Bone health and osteoporosis management of the patient with Duchenne muscular dystrophy. *Pediatrics.* 2018;142(Suppl 2):S34-42.

16. Chang M, Cai Y, Gao Z, Chen X, Liu B, Zhang C, et al. Duchenne muscular dystrophy: pathogenesis and promising therapies. *J Neurol*. 2023;270:3733–49.
17. Mendell JR, Shieh PB, McDonald CM, Sahenk Z, Lehman KJ, Lowes LP, et al. Expression of SRP-9001 dystrophin and stabilization of motor function up to 2 years post-treatment with delandistrogene moxeparvovec gene therapy in individuals with Duchenne muscular dystrophy. *Front Cell Dev Biol*. 2023;11:1167762.
18. Clemens PR, Rao VK, Connolly AM, Harper AD, Mah JK, McDonald CM, et al. Efficacy and safety of viltolarsen in boys with Duchenne muscular dystrophy: results from the Phase 2, open-label, 4-year extension study. *J Neuromuscul Dis*. 2023;10:439–47.
19. Frank DE, Schnell FJ, Akana C, El-Husayni SH, Desjardins CA, Morgan J, et al. Increased dystrophin production with golodirsen in patients with Duchenne muscular dystrophy. *Neurology*. 2020;94:e2270–82.
20. Iff J, Gerrits C, Zhong Y, Tuttle E, Birk E, Zheng Y, et al. Delays in pulmonary decline in eteplirsen-treated patients with Duchenne muscular dystrophy. *Muscle Nerve*. 2022;66:262–9.
21. Wagner KR, Kuntz NL, Koenig E, East L, Upadhyay S, Han B, et al. Safety, tolerability, and pharmacokinetics of casimersen in patients with Duchenne muscular dystrophy amenable to exon 45 skipping: a randomized, double-blind, placebo-controlled, dose-titration trial. *Muscle Nerve*. 2021;64:285–92.
22. Forrest S, Meloni PL, Muntoni F, Kim J, Fletcher S, Wilton SD. Personalized exon skipping strategies to address clustered non-deletion dystrophin mutations. *Neuromuscul Disord*. 2010;20:810–6.
23. Akat A, Karaöz E. Cell therapy strategies on Duchenne muscular dystrophy: a systematic review of clinical applications. *Stem Cell Rev Rep*. 2023;20(1):138–58.
24. Sun C, Serra C, Lee G, Wagner KR. Stem cell-based therapies for Duchenne muscular dystrophy. *Exp Neurol*. 2020;323: 113086.
25. Cerletti M, Jurga S, Witczak CA, Hirshman MF, Shadrach JL, Goodyear LJ, et al. Highly efficient, functional engraftment of skeletal muscle stem cells in dystrophic muscles. *Cell*. 2008;134:37–47.
26. Darabi R, Arpke RW, Irion S, Dimos JT, Grskovic M, Kyba M, et al. Human ES- and iPS-derived myogenic progenitors restore dystrophin and improve contractility upon transplantation in dystrophic mice. *Cell Stem Cell*. 2012;10:610–9.
27. He R, Li H, Wang L, Li Y, Zhang Y, Chen M, et al. Engraftment of human induced pluripotent stem cell-derived myogenic progenitors restores dystrophin in mice with duchenne muscular dystrophy. *Biol Res*. 2020;53:22.
28. Tedesco FS, Hoshiya H, D'Antona G, Gerli MF, Messina G, Antonini S, et al. Stem cell-mediated transfer of a human artificial chromosome ameliorates muscular dystrophy. *Sci Transl Med*. 2011;3:96ra578.
29. Zhao M, Tazumi A, Takayama S, Takenaka-Ninagawa N, Nalbandian M, Nagai M, et al. Induced fetal human muscle stem cells with high therapeutic potential in a mouse muscular dystrophy model. *Stem Cell Rep*. 2020;15:80–94.
30. Takenaka-Ninagawa N, Goto M, Bourgeois-Yoshioka CK, Miki M, Sakurai H. Cell therapy for duchenne muscular dystrophy using induced pluripotent stem cell-derived muscle stem cells and the potential of regenerative rehabilitation. *Curr Opin Biomed Eng*. 2024;30:100523.
31. Malik M, Siemionow M, Cwykiel J, Heydemann A, Garcia-Martinez J, Siemionow K, et al. Intraosseous transplant of dystrophin expressing chimeric (DEC) cells improves skeletal muscle function in mdx mouse model of Duchenne muscular dystrophy. *Postepy Kardiol Interwencyjne*. 2022;18:399–406.
32. Iyer PS, Mavoungou LO, Ronzoni F, Zemla J, Schmid-Siegert E, Antonini S, et al. Autologous cell therapy approach for Duchenne muscular dystrophy using PiggyBac transposons and mesoangioblasts. *Mol Ther*. 2018;26:1093–108.
33. Xie N, Chu SN, Azzag K, Schultz CB, Peifer LN, Kyba M, et al. *In vitro* expanded skeletal myogenic progenitors from pluripotent stem cell-derived teratomas have high engraftment capacity. *Stem Cell Rep*. 2021;16:2900–12.
34. Siemionow M, Langa P, Brodowska S, Kozłowska K, Zalants K, Budzynska K, et al. Long-term protective effect of human dystrophin expressing chimeric (DEC) cell therapy on amelioration of function of cardiac, respiratory and skeletal muscles in Duchenne muscular dystrophy. *Stem Cell Rev Rep*. 2022;18:2872–92.
35. Ricotti V, Ridout DA, Pane M, Main M, Mayhew A, Mercuri E, et al. The NorthStar ambulatory assessment in Duchenne muscular dystrophy: considerations for the design of clinical trials. *J Neurol Neurosurg Psychiatry*. 2016;87:149–55.
36. Shiomi K, Kiyono T, Okamura K, Uezumi M, Goto Y, Yasumoto S, et al. CDK4 and cyclin D1 allow human myogenic cells to recapture growth property without compromising differentiation potential. *Gene Ther*. 2011;18:857–66.
37. Kudoh H, Ikeda H, Kakitani M, Ueda A, Hayasaka M, Tomizuka K, et al. A new model mouse for Duchenne muscular dystrophy produced by 2.4-Mb deletion of dystrophin gene using Cre-loxP recombination system. *Biochem Biophys Res Commun*. 2005;328:507–16.
38. Yamamoto M, Kim M, Imai H, Itakura Y, Ohtsuki G. Microglia-triggered plasticity of intrinsic excitability modulates psychomotor behaviors in acute cerebellar inflammation. *Cell Rep*. 2019;28:2923–2938.e8.
39. Nakano M, Imamura H, Nagai T, Noji H. Ca²⁺ regulation of mitochondrial ATP synthesis visualized at the single cell level. *ACS Chem Biol*. 2011;6:709–15.
40. Itoh Y, Murakami T, Mori T, Agata N, Kimura N, Inoue-Miyazu M, et al. Training at non-damaging intensities facilitates recovery from muscle atrophy. *Muscle Nerve*. 2017;55:243–53.
41. Matsuda R, Nishikawa A, Tanaka H. Visualization of dystrophic muscle fibers in mdx mouse by vital staining with Evans blue: evidence of apoptosis in dystrophin-deficient muscle. *J Biochem*. 1995;118:959–64.
42. Choi J, Matoba N, Setoyama D, Watanabe D, Ohnishi Y, Yasui R, et al. The SGLT2 inhibitor empagliflozin improves cardiac energy status via mitochondrial ATP production in diabetic mice. *Commun Biol*. 2023;6:278.
43. Krivickas LS, Dorer DJ, Ochala J, Frontera WR. Relationship between force and size in human single muscle fibres. *Exp Physiol*. 2011;96:539–47.
44. Webster C, Silberstein L, Hays AP, Blau HM. Fast muscle fibers are preferentially affected in Duchenne muscular dystrophy. *Cell*. 1988;52:503–13.
45. Schiaffino S, Reggiani C. Fiber types in mammalian skeletal muscles. *Physiol Rev*. 2011;91:1447–531.
46. Talbot J, Maves L. Skeletal muscle fiber type: using insights from muscle developmental biology to dissect targets for susceptibility and resistance to muscle disease. *Wiley Interdiscip Rev Dev Biol*. 2016;5:518–34.
47. Choi SJ. Differential susceptibility on myosin heavy chain isoform following eccentric-induced muscle damage. *J Exerc Rehabil*. 2014;10:344–8.
48. Mukund K, Subramaniam S. Skeletal muscle: a review of molecular structure and function, in health and disease. *Wiley Interdiscip Rev Syst Biol Med*. 2020;12: e1462.
49. Siemionow M, Langa P, Harasymczuk M, Cwykiel J, Siewlewicz M, Smieszek J, et al. Human dystrophin expressing chimeric (DEC) cell therapy ameliorates cardiac, respiratory, and skeletal muscle's function in Duchenne muscular dystrophy. *Stem Cells Transl Med*. 2021;10:1406–18.
50. Siemionow M, Cwykiel J, Heydemann A, Garcia-Martinez J, Siemionow K, Szilagyi E. Creation of dystrophin expressing chimeric cells of myoblast origin as a novel stem cell based therapy for Duchenne muscular dystrophy. *Stem Cell Rev Rep*. 2018;14:189–99.
51. Maurissen JP, Marable BR, Andrus AK, Stebbins KE. Factors affecting grip strength testing. *Neurotoxicol Teratol*. 2003;25:543–53.
52. Benchaouir R, Meregalli M, Farini A, D'Antona G, Belicchi M, Goyenvalle A, et al. Restoration of human dystrophin following transplantation of exon-skipping-engineered DMD patient stem cells into dystrophic mice. *Cell Stem Cell*. 2007;1:646–57.
53. Perrino C, Gargiulo G, Pironti G, Franzone A, Scudiero L, De Laurentis M, et al. Cardiovascular effects of treadmill exercise in physiological and pathological preclinical settings. *Am J Physiol Heart Circ Physiol*. 2011;300:H1983–9.
54. Birnkrant DJ, Carter JC. Back to basics: the respiratory management of Duchenne muscular dystrophy. *Thorax*. 2022;77:743–4.
55. McDonald CM, Henricson EK, Han JJ, Abresch RT, Nicorici A, Elfving GL, et al. The 6-minute walk test as a new outcome measure in Duchenne muscular dystrophy. *Muscle Nerve*. 2010;41:500–10.
56. McGreevy JW, Hakim CH, McIntosh MA, Duan D. Animal models of Duchenne muscular dystrophy: from basic mechanisms to gene therapy. *Dis Model Mech*. 2015;8:195–213.
57. Tanaka H, Hayashi K, Ozawa E. Positive immunostaining with dystrophin antibodies in mdx skeletal muscle. *Proc Jpn Acad Ser B*. 1991;67:148–52.
58. Frinchi M, Morici G, Mudó G, Bonsignore MR, Di Liberto V. Beneficial role of exercise in the modulation of mdx muscle plastic remodeling and oxidative stress. *Antioxidants (Basel)*. 2021;10(4):558.

59. Hyzewicz J, Ruegg UT, Takeda S. Comparison of experimental protocols of physical exercise for mdx mice and duchenne muscular dystrophy patients. *J Neuromuscul Dis.* 2015;2:325–42.
60. Suetterlin KJ, Männikkö R, Matthews E, Greensmith L, Hanna MG, Bostock H, et al. Excitability properties of mouse and human skeletal muscle fibres compared by muscle velocity recovery cycles. *Neuromuscul Disord.* 2022;32:347–57.
61. Incitti T, Magli A, Jenkins A, Lin K, Yamamoto A, Perlingeiro RCR. Pluripotent stem cell-derived skeletal muscle fibers preferentially express myosin heavy-chain isoforms associated with slow and oxidative muscles. *Skelet Muscle.* 2020;10:17.
62. Yasuda T, Ishihara T, Ichimura A, Ishihara N. Mitochondrial dynamics define muscle fiber type by modulating cellular metabolic pathways. *Cell Rep.* 2023;42: 112434.
63. Lanza IR, Nair KS. Mitochondrial metabolic function assessed in vivo and in vitro. *Curr Opin Clin Nutr Metab Care.* 2010;13:511–7.
64. Rybalka E, Timpani CA, Cooke MB, Williams AD, Hayes A. Defects in mitochondrial ATP synthesis in dystrophin-deficient mdx skeletal muscles may be caused by complex I insufficiency. *PLoS ONE.* 2014;9: e115763.
65. Percival JM, Siegel MP, Knowels G, Marcinek DJ. Defects in mitochondrial localization and ATP synthesis in the mdx mouse model of Duchenne muscular dystrophy are not alleviated by PDES inhibition. *Hum Mol Genet.* 2013;22:153–67.
66. Siegel MP, Kruse SE, Knowels G, Salmon A, Beyer R, Xie H, et al. Reduced coupling of oxidative phosphorylation *in vivo* precedes electron transport chain defects due to mild oxidative stress in mice. *PLoS ONE.* 2011;6: e26963.
67. Timpani CA, Hayes A, Rybalka E. Revisiting the dystrophin-ATP connection: how half a century of research still implicates mitochondrial dysfunction in Duchenne muscular dystrophy aetiology. *Med Hypotheses.* 2015;85:1021–33.
68. Barton-Davis ER, Cordier L, Shoturma DI, Leland SE, Sweeney HL. Aminoglycoside antibiotics restore dystrophin function to skeletal muscles of mdx mice. *J Clin Invest.* 1999;104:375–81.
69. Godfrey C, Muses S, McClorey G, Wells KE, Coursindel T, Terry RL, et al. How much dystrophin is enough: the physiological consequences of different levels of dystrophin in the mdx mouse. *Hum Mol Genet.* 2015;24:4225–37.
70. Sharp PS, Bye-a-Jee H, Wells DJ. Physiological characterization of muscle strength with variable levels of dystrophin restoration in mdx mice following local antisense therapy. *Mol Ther.* 2011;19:165–71.
71. van Putten M, Hulsker M, Nadarajah VD, van Heiningen SH, van Huizen E, van Iterson M, et al. The effects of low levels of dystrophin on mouse muscle function and pathology. *PLoS ONE.* 2012;7: e31937.
72. van den Bergen JC, Wokke BH, Janson AA, van Duinen SG, Hulsker MA, Ginjaar HB, et al. Dystrophin levels and clinical severity in Becker muscular dystrophy patients. *J Neurol Neurosurg Psychiatry.* 2014;85:747–53.
73. Cardone N, Taglietti V, Baratto S, Kefi K, Periou B, Gitiaux C, et al. Myopathologic trajectory in Duchenne muscular dystrophy (DMD) reveals lack of regeneration due to senescence in satellite cells. *Acta Neuropathol Commun.* 2023;11:167.
74. Wada MR, Inagawa-Ogashiwa M, Shimizu S, Yasumoto S, Hashimoto N. Generation of different fates from multipotent muscle stem cells. *Development.* 2002;129:2987–95.

Publisher's Note

Springer Nature remains neutral with regard to jurisdictional claims in published maps and institutional affiliations.